Transcriptome-wide analysis of the function of Ded1 in translation preinitiation complex assembly in a reconstituted in vitro system

Fujun Zhou[1], Julie M. Bocetti[1]*, Meizhen Hou[1]*, Daoming Qin[3]*, Alan G. Hinnebusch[2†] and Jon R. Lorsch[1†]

[1]Section on the Mechanism and Regulation of Protein Synthesis
Eunice Kennedy Shriver National Institute of Child Health and Human Development
National Institutes of Health
Bethesda, MD USA

[2]Section on Nutrient Control of Gene Expression
Eunice Kennedy Shriver National Institute of Child Health and Human Development
National Institutes of Health
Bethesda, MD USA

*Equal contributions

[†]Corresponding Author

[3]Current address: Steamify LLC, Mclean, VA USA

ABSTRACT

We have developed a deep sequencing-based approach, Rec-Seq, that allows simultaneous monitoring of ribosomal 48S pre-initiation complex (PIC) formation on every mRNA in the translatome in an in vitro reconstituted system. Rec-Seq isolates key early steps in translation initiation in the absence of all other cellular components and processes. Using this approach we show that the DEAD-box ATPase Ded1 promotes 48S PIC formation on the start codons of >1000 native mRNAs, most of which have long, structured 5'-untranslated regions (5'UTRs). Remarkably, initiation measured in Rec-Seq was enhanced by Ded1 for most mRNAs previously shown to be highly Ded1-dependent by ribosome profiling of *ded1* mutants in vivo, demonstrating that the core translation functions of the factor are recapitulated in the purified system. Our data do not support a model in which Ded1acts by reducing initiation at alternative start codons in 5'UTRs and instead indicate it functions by directly promoting mRNA recruitment to the 43S PIC and scanning to locate the main start codon. We also provide evidence that eIF4A, another essential DEAD-box initiation factor, is required for efficient PIC assembly on almost all mRNAs, regardless of their structural complexity, in contrast to the preferential stimulation by Ded1 of initiation on mRNAs with long, structured 5'UTRs.

41 **INTRODUCTION**

42 Translation initiation in eukaryotes begins with the assembly of the 43S preinitiation
43 complex (PIC), containing the small (40S) ribosomal subunit bound to the eIF2•GTP•Met-
44 $tRNA_i$ ternary complex and several initiation factors (eIFs), including eIF1, eIF1A, eIF5, eIF4B,
45 and eIF3. The 43S PIC binds the 5' end of m^7G-capped mRNAs with the assistance of the cap-
46 binding protein complex eIF4F, comprised of cap-binding subunit eIF4E, scaffolding and
47 mRNA-binding subunit eIF4G, and DEAD-box RNA helicase eIF4A. The resulting 43S•mRNA
48 complex, or 48S PIC, scans the 5'-untranslated region (5'UTR) for a suitable start codon, whose
49 selection triggers release of most of the initiation factors. Subsequent joining of the large (60S)
50 ribosomal subunit to the 40S•Met-$tRNA_i$ complex, with the aid of eIF1A and the GTPase factor
51 eIF5B, forms the 80S initiation complex, poised to begin the elongation phase of protein
52 synthesis (Hinnebusch 2014).

53 The efficiency of translation initiation on specific mRNAs is strongly influenced by the
54 secondary structures in the 5'UTR and the length of the 5'UTR (Sonenberg and Hinnebusch
55 2009; Niederer et al. 2022). It is believed that the inhibitory structures in mRNA 5'UTRs are
56 resolved by DEAD/H-box RNA helicases (Hinnebusch 2014). However, we and others have
57 demonstrated that eIF4A is required for the efficient recruitment of a variety of mRNAs tested in
58 vitro regardless of their degrees of structure (Pestova and Kolupaeva 2002; Yourik et al. 2017).
59 Consistent with this, profiling of translating 80S ribosomes in vivo (Ribo-Seq analysis) in an
60 eIF4A temperature-sensitive yeast mutant (*tif1-ts*) revealed that eIF4A inactivation reduced the
61 relative translation efficiencies of less than 40 mRNAs, despite a strong reduction in bulk
62 polysome assembly (Sen et al. 2015), thus suggesting that the majority of mRNAs have similarly
63 strong requirements for eIF4A in yeast cells. Mammalian eIF4A has been suggested to remodel

64 the 40S subunit to enhance PIC attachment to mRNAs and function beyond its role in RNA
65 unwinding (Sokabe and Fraser 2017) and might facilitate the threading of the 5′-end of mRNA
66 into the 40S entry channel (Kumar et al. 2016).

67 In contrast to eIF4A, inactivation of yeast DEAD-box helicase Ded1 in a cold-sensitive
68 mutant (*ded1-cs*) was found to reduce the relative TEs of more than 1100 mRNAs in Ribo-Seq
69 experiments (Sen et al. 2015; Sen et al. 2019). These Ded1-hyperdependent mRNAs displayed a
70 marked tendency for long and structured 5'UTRs (Sen et al. 2015). Profiling of small (40S)
71 ribosomal subunits in the *ded1-cs* mutant provided evidence that Ded1 stimulates the translation
72 of Ded1-hyper-dependent mRNAs by promoting attachment of 43S PICs to the mRNA 5'ends or
73 subsequent scanning to the start codon (Sen et al. 2019). Furthermore, in a purified yeast
74 translation initiation system several mRNAs identified as being hyperdependent on Ded1 in vivo
75 also displayed greater stimulation by Ded1 of 48S PIC assembly than observed for either Ded1-
76 hypodependent mRNAs or variants of the hyperdependent mRNAs lacking their 5'UTR
77 secondary structures (Gupta et al. 2018). Together, these findings suggest that Ded1 is important
78 particularly for stimulating translation of mRNAs that have long, structured 5'UTRs. Several
79 lines of evidence indicate that Ded1 activity on such mRNAs is enhanced by interaction of its N-
80 terminal domain with eIF4A and eIF4E, and of its C-terminal domain with eIF4G (Gao et al.
81 2016; Gupta et al. 2018; Gulay et al. 2020), indicating functional coupling between eIF4F and
82 Ded1 in 48S PIC assembly. Other evidence suggests that Ded1 broadly promotes scanning
83 through 5'UTRs by blocking initiation at alternative start codons positioned just upstream of
84 secondary structures that are unwound by Ded1 in vivo, thus allowing the scanning PIC to
85 continue downstream to the main start codon of the mRNA (Guenther et al. 2018).

86 It appears that Ded1 can regulate translation of mRNAs in vivo in ways ostensibly
87 distinct from its functions in promoting PIC attachment or scanning on structured mRNAs. Ded1
88 and its mammalian ortholog DDX3 have been implicated in facilitating the joining of the large
89 ribosomal subunit to the 48S PIC after start codon recognition (Geissler et al. 2012; Wang et al.
90 2022). There is also evidence that Ded1 can repress translation by segregating mRNAs into
91 phase-separated RNA–protein granules, processing bodies (PBs) or stress granules (SGs), during
92 cell stresses. Granule formation in glucose-starved cells is reduced by depletion of Ded1, and is
93 enhanced by Ded1 overexpression or impairment of its ATPase activity in non-starved cells in a
94 manner regulated by regions in the Ded1 NTD and CTD (Beckham et al. 2008; Hilliker et al.
95 2011; Hondele et al. 2019). It was suggested that Ded1 initially forms an inactive complex with
96 eIF4F and mRNA that is stalled at a step upstream of 43S PIC joining and subsequently utilizes
97 ATP hydrolysis to allow progression into the initiation pathway (Beckham et al. 2008; Hilliker et
98 al. 2011).
99 Heat-shock also evokes Ded1 sequestration in SGs in a manner antagonized at low
100 temperatures by a polar intrinsically disordered region (IDR) in the Ded1 NTD. Purified Ded1
101 displayed heat-induced phase separation in vitro that was enhanced by mRNA and the Ded1
102 CTD but suppressed by the N-terminal IDR. Interestingly, heat-shock preferentially reduced the
103 TEs of mRNAs with structured 5' UTRs and increased their condensation, in a manner
104 modulated by the N-terminal IDR, leading to the model that condensation of Ded1 and
105 associated mRNAs preferentially reduces the translation of Ded1-hyperdependent mRNAs with
106 structured 5'UTRs during heat-shock (Iserman et al. 2020). Other findings indicate that glucose-
107 starvation or heat-shock leads to widespread dissociation of Ded1, eIF4A and eIF4B from the
108 5'UTRs of mRNAs (Castelli et al. 2011; Bresson et al. 2020), which could underlie reduced

109 translation of Ded1-hyperdependent mRNAs that remain soluble in stressed cells. Examining
110 the TE changes conferred by glucose starvation or heat-shock by ribosome profiling suggested
111 that Ded1-hyperdependent mRNAs vary greatly in their translational suppression during stress,
112 which might involve a combinatorial effect of impairing eIF4A, eIF4B, and Ded1 function on the
113 most affected subsets (Sen et al. 2021).

114 It is possible that Ded1 has additional functions in the nucleus, as it appears to shuttle
115 between nucleus and cytoplasm and interacts both physically and functionally with the nuclear
116 cap-binding proteins (Senissar et al. 2014). Ded1 was also found to co-purify with pre-90S and
117 pre-40S immature ribosomes (Schäfer et al. 2003), and thus might function in ribosome
118 biogenesis.

119 A difficulty with interpreting the previous ribosome profiling experiments with *ded1*
120 mutations is that the inactivated mutant protein could have had dominant effects rather than
121 simply producing a loss of Ded1 function. For example, in view of evidence that inhibition of
122 Ded1 ATPase activity can lead to the formation of translationally inert mRNP granules, it is
123 possible that the *ded1* mutations in the catalytic domain analyzed by ribosome profiling led to
124 impaired translation of many Ded1-hyperdependent mRNAs in non-stressed cells owing to their
125 sequestration with the mutant *ded1* proteins in condensates inaccessible to the initiation
126 machinery. It was also possible that the inactivated mutant proteins bound to mRNAs, the
127 ribosome or other initiation factors in a manner that inhibited translation. The *ded1* mutations
128 could also indirectly impair translation of Ded1-hyperdependent mRNAs by reducing their
129 export from the nucleus, by reducing expression of another protein with a role in production or
130 function of the translation initiation machinery, by activating stress responses that alter the
131 functions of initiation factors, or by eliciting quality control responses that alter the rate of

132 translation elongation. Even wild-type Ded1 could influence translation indirectly by
133 modulating the association of various RNA-binding proteins with mRNAs, a function ascribed to
134 other DEAD-box proteins (Linder and Jankowsky 2011). As noted above, we demonstrated that
135 several mRNAs that were found to be Ded1-hyperdependent in vivo displayed a greater
136 stimulation of 48S PIC assembly by Ded1 compared to several in vivo hypodependent mRNAs
137 in a fully purified system, confirming a direct role of Ded1 in stimulating initiation on these few
138 mRNAs in the soluble phase in the absence of any other cellular proteins besides ribosomes and
139 canonical initiation factors. However, it was possible that many other mRNAs found to be
140 hyperdependent on Ded1 in vivo are not stimulated directly by Ded1's ability to resolve
141 secondary structures in 5'UTRs and promote PIC recruitment or scanning to the start codon.
142 We have developed an elaboration of the reconstituted yeast translation initiation system
143 (Acker et al. 2007) that enables examination of 48S PIC assembly on all native yeast mRNAs
144 simultaneously. This approach, dubbed Recruitment-Sequencing (Rec-Seq), allowed us to
145 measure direct effects of Ded1 on PIC attachment to mRNA and scanning to the start codon in
146 reactions containing only 40S ribosomal subunits, methionyl-initiator tRNA (Met-tRNA$_i$),
147 GDPNP and ATP, and the core initiation factors. In previous work using the reconstituted yeast
148 initiation system, we found that stable 48S PIC formation on mRNA start codons was strongly
149 dependent on the 5'-cap (Mitchell et al. 2010; Yourik et al. 2017). The cap also prevented off-
150 pathway events and enforced a requirement for the full set of initiation factors to efficiently
151 assemble a 48S PIC. These results indicate that in the reconstituted system 43S PICs are loaded
152 onto the 5'-ends of mRNAs in a cap-dependent manner and that they scan from 5' to 3' to locate
153 the start codon.

154 Rec-Seq allowed us to isolate the crucial and highly regulated series of events leading up
155 to 48S PIC assembly from all later steps of initiation and elongation. Processes such as mRNA
156 localization and decay and RNA and protein compartmentalization, which can complicate in
157 vivo analyses, likewise do not contribute to the outcome of Rec-Seq experiments. Because we
158 could vary Ded1 concentration in reactions, or leave it out entirely, Rec-Seq allowed us to
159 directly interrogate the factor's role instead of relying on inferences from the effects of *ded1*
160 mutations. Moreover, we could evaluate whether preventing initiation at alternative start codons
161 in 5'UTRs is an important aspect of Ded1 enhancement of PIC assembly at the canonical start
162 codons on Ded1-stimulated transcripts in vitro.

163 Our studies indicate that in the Rec-Seq system Ded1 stimulates 48S PIC assembly on
164 ~1000 mRNAs. These Ded1-dependent mRNAs include ~90% of the mRNAs previously found
165 to be hyperdependent on Ded1 in vivo by ribosome profiling of the *ded1-cs* mutant. The fact that
166 addition of Ded1 stimulates 48S PIC assembly on these mRNAs in the reconstituted Rec-Seq
167 system argues against the involvement of other cellular processes or proteins beyond the core
168 initiation machinery in Ded1 function, and the possibility that the in vivo ribosome profiling
169 results were influenced by dominant negative effects of the *ded1-cs* mutation or by altered
170 expression or activity of the translational machinery in the mutant cells. The mRNAs that are
171 strongly dependent on Ded1 in the Rec-Seq system exhibit a high propensity for long and
172 structured 5'UTRs, providing compelling evidence that Ded1 acts directly to stimulate 48S PIC
173 formation by unwinding 5'UTR structures to facilitate mRNA binding to the PIC and scanning to
174 find the start codon. Our results also indicate that alternative initiation at upstream start codons is
175 too infrequent, and the suppression of these events by addition of Ded1 too small, to account for
176 the stimulatory effects of Ded1 on 48S PIC assembly in the reconstituted system. Finally, we

177 show that eIF4A strongly stimulates the formation of 48S PICs on the vast majority of yeast
178 mRNAs, regardless of their 5'UTR length or degree of secondary structure, in contrast to the
179 specificity we observe for Ded1 in stimulating recruitment of mRNAs with long, structured
180 5'UTRs. These data are consistent with the model that eIF4A plays a general role in facilitating
181 binding of all mRNAs to the 43S PIC, whereas Ded1 unwinds inhibitory secondary structures to
182 promote PIC binding and scanning on mRNAs with structured 5'UTRs.
183

184 **RESULTS**

185 **Rec-Seq, an in vitro approach to measure 48S PIC formation transcriptome-wide.** We
186 previously developed a fully reconstituted yeast translation initiation system (Acker et al. 2007)
187 that allows measurement of stable recruitment of mRNAs to 43S pre-initiation complexes
188 (Mitchell et al. 2010) to form 48S PICs using defined concentrations of purified components for
189 individual mRNAs. In addition to purified small (40S) ribosomal subunits, reactions include
190 initiation factors eIF1, eIF1A, eIF5, the eIF2·GTP·Met-tRNA$_i$ ternary complex (TC, assembled
191 using non-hydrolyzable GDPNP), eIF3, the mRNA-recruitment factors eIF4G·eIF4E complex,
192 eIF4A and eIF4B, and ATP. In the initial version of this system, we monitored recruitment of a
193 single capped, radiolabeled, in vitro transcribed mRNA in each reaction. Formation of a stable
194 48S PIC with the anticodon of Met-tRNA$_i$ base paired to the AUG start codon in the mRNA was
195 resolved from free mRNA by native gel electrophoresis and quantified by phosphorimaging of
196 the mRNA. Among other things, this assay has been used to elucidate the molecular roles of eIFs
197 essential for 48S PIC assembly (Hinnebusch 2014); provide evidence that eIF4A is essential for
198 recruitment of various mRNAs to the 43S PIC regardless of the amount of secondary structure in
199 their 5'UTRs (Yourik et al. 2017); and reconstitute the ability of Ded1 to overcome 5'UTR

200 secondary structures found in several Ded1-hyperdependent mRNAs (Gupta et al. 2018). An
201 important limitation of the assay, however, was that only a single mRNA could be examined at a
202 time, and the effects of competition among the many different mRNAs that exist in a cell could
203 not be assessed. In addition, the use of an electrophoretic mobility-shift assay (EMSA) limits the
204 analysis to very short native transcripts, eg. *RPL41A* mRNA, or the use of synthetic constructs
205 truncated at their 3' ends in place of longer, full-length native mRNAs (Gupta et al. 2018). Such
206 constructs might not recapitulate functionally important interactions between the 5'UTR and
207 other parts of the mRNA.

208 To circumvent these limitations, we modified the system to allow 48S PIC formation on
209 all native mRNAs in the standard yeast transcriptome to be monitored simultaneously using an
210 approach we call Rec-Seq for "Recruitment-Sequencing" (Fig. 1A). In place of a single,
211 radiolabeled mRNA we used oligo(dT) affinity-purified total mRNA from wild-type yeast cells
212 grown in nutrient-replete conditions. This total polyA(+) mRNA was incubated for various times
213 with pre-assembled 43S PICs, eIF3, eIF4 factors, ATP and other components (depending on the
214 experiment; Fig. 1-S1). The reactions were then treated with RNase I to digest mRNA regions
215 not protected by the ribosomal complex. For each reaction, 48S PICs were isolated by
216 sedimentation through a sucrose gradient and ribosome-protected fragments (RPFs) were
217 purified by gel electrophoresis and converted to cDNAs by reverse-transcription followed by
218 PCR amplification to generate sequencing libraries. This approach allowed us to monitor PIC
219 assembly on all native yeast mRNAs in parallel.

220 To make results comparable among replicates and across experiments, we used an
221 internal normalization approach in which 48S PICs were assembled on two non-native mRNAs
222 encoding Renilla or firefly luciferase and treated with RNase I. A constant amount of these

223 “spike-in” 48S PICs were added to each experimental reaction prior to sucrose gradient
224 sedimentation (Fig. 1-S2A). RPFs corresponding to both the main AUG (mAUG) and several
225 internal AUGs (iAUGs) were found to be highly reproducible among biological replicates for
226 these spike-in controls (Fig. 1-S2B-D). Normalizing results with these control RPFs allowed us
227 to achieve high reproducibility among triplicate biological replicate experiments (Fig. 1-S3) and
228 also allowed us to measure absolute rather than relative 48S PIC formation efficiencies despite
229 differences in final read depths from reaction to reaction.

230 To assess the function of Ded1 in mRNA recruitment, scanning and start codon
231 recognition, we carried out Rec-Seq experiments on reactions that contained all of the canonical
232 initiation factors shown in Figure 1A (including eIF4A) and either lacked Ded1 or contained 100
233 or 500 nM Ded1. The reactions were initiated by adding total polyA(+) mRNA to the pre-formed
234 43S complexes and other factors, and then quenched rapidly after 15 min by
235 depleting ATP with addition of a “Stop buffer” containing hexokinase and glucose. We chose 15
236 minutes because recruitment has reached its observed endpoint for nearly all mRNAs at this
237 time. The RPFs thus measured give the final distribution of competitive recruitment efficiencies
238 under these experimental conditions, in which there is a two-fold excess of total mRNA over 43S
239 PICs. After sequencing cDNA libraries prepared from the RNAse I-treated purified 48S PICs
240 and removing sequencing reads mapping to non-coding RNAs, the reads mapping to protein
241 coding sequences were examined.

242 A metagene plot of the number of RPF reads versus position of RPF 5’ends relative to the
243 mAUG codon for each mRNA revealed that the overwhelming majority contain a single peak of
244 RPFs with the bulk of 5’ ends located 12 nt upstream of the mAUG codon (Fig. 1B-D). This is
245 the position expected for PICs with the 40S P site containing the AUG start codon base paired

246 with the anticodon of Met-tRNA$_i$ (Ingolia et al. 2009; Archer et al. 2016). A minority of RPFs
247 have 5'ends closer to the AUG codon (Fig. 1B-D), which could result from invasion of RNase I
248 into the 40S exit channel in a minor fraction of PICs positioned at the start codon, or from low-
249 level degradation of purified RPFs during library construction. The two reactions containing
250 Ded1 have a somewhat greater abundance of RPFs at the start codons compared to the reaction
251 lacking Ded1 (Fig. 1-S4A).

252 We examined individual Rec-Seq traces for several mRNAs previously shown through
253 ribosome profiling to be either hyper- or hypo-dependent on Ded1 for translational efficiency
254 and that had also been shown to be similarly dependent on Ded1 for 43S PIC recruitment in vitro
255 in the reconstituted yeast initiation system (Fig. 1E, F; Fig. 1S-4). The Ded1 hyper-dependent
256 mRNAs showed strong Ded1-enhancement of Rec-Seq RPF peaks mapping to the mAUG (Fig.
257 1S-4B-E), as exemplified for *OST3* in Fig. 1E. In contrast, mRNAs previously shown to be
258 hypo-dependent on Ded1 by ribosome profiling, including *HOR7* (Fig. 1F), showed modest
259 stimulation, no enhancement, or even diminished RPF counts at the mAUG in reactions
260 containing 100 or 500 nM Ded1 vs. no Ded1 (Fig. 1S-4F-I).

261 We conducted differential expression analysis using the software DESeq2 (Love et al.
262 2014) to identify mRNAs that exhibit statistically significant changes in normalized RPFs
263 mapping to the main start codon (mRPFs) on addition of Ded1. Groups of ~1000 transcripts
264 among the 3052 for which Rec-Seq data were obtained showed >2-fold increased mRPFs in the
265 presence of 100 or 500 nM Ded1 compared to no added Ded1, whereas only ~100 transcripts
266 showed higher mRPFs at 500 nM versus 100 nM Ded1 (Fig. 2A-C, red dots). Substantially
267 smaller numbers of mRNAs displayed decreased mRPFs as Ded1 concentration was increased
268 (Fig. 2A-C, dark blue dots; 71, 182 and 51 mRNAs, respectively). Importantly, 87% of mRNAs

269 showing significant increases in mRPFs at 100 nM Ded1 were also increased at 500 nM Ded1
270 (Fig. 2D), and 68% of the mRNAs with significantly diminished mRPFs at 100 nM Ded1 were
271 also decreased at 500 nM Ded1 (Fig. 2E)—both highly significant overlaps. These data indicate
272 consistency in the effects of Ded1 observed in different experiments. The 1006 mRNAs with
273 significantly increased mRPFs at 500 nM Ded1 had median increases of 3.6-fold and 4.8-fold at
274 100 nM and 500 nM Ded1, respectively (Fig. 2F, cols. 3-4). Similarly, the 911 mRNAs that had
275 significantly increased mRPFs in 100 nM Ded1 had median increases of 4.1-fold and 5.2-fold at
276 100 nM and 500 nM Ded1, respectively, and the 793 mRNAs common to both sets had median
277 increases of 4.7-fold and 6.1-fold (Fig. 2F, cols. 5-8). Although the greater median stimulation
278 at 500 nM vs. 100 nM Ded1 is significant for all three mRNA groups, these results indicate that
279 100 nM Ded1 is nearly saturating for enhancement of 48S PIC assembly for the majority of
280 Ded1-stimulated mRNAs in the in vitro system.

281 The set of mRNAs displaying diminished mRPFs at 500 nM Ded1 showed smaller
282 reductions at 100 nM (Fig. 2F, cols. 9-10; median mRPF changes of 0.59 vs. 0.37 at 100 nM and
283 500 nM Ded1, respectively), indicating that the inhibitory effect of Ded1 on these mRNAs is not
284 saturated at the lower concentration. For the remaining two groups that showed Ded1
285 suppression of mRPFs at 100 nM or both 100nM and 500 nM Ded1, the median degree of Ded1
286 inhibition did not differ significantly between the two concentrations (Fig. 2F, cols. 11-14),
287 indicating that inhibition by Ded1 was saturated at 100 nM.

288 The mRPF reads for each gene were normalized to the total RNA reads across the coding
289 sequences (CDS) of the mRNA (normalized for CDS length)—a measure of transcript
290 abundance—to calculate the recruitment efficiency (RE) of each transcript. The RE is analogous
291 to translational efficiency (TE) determined by in vivo Ribo-Seq experiments. We examined

292 changes in RE between experiments containing different concentrations of Ded1 by ordering
293 mRNAs according to the change in RE between 0 and 100 nM Ded1 and then using this ordering
294 to generate a heat-map depiction of ΔRE values for all 3052 transcripts observed by Rec-Seq
295 between 0 and 100 nM Ded1, 0 and 500 nM Ded1, and 100 and 500 nM Ded1 (Fig. 2G).
296 Consistent with Figures 2D and E, the results indicate that most mRNAs with increased REs on
297 addition of 100 nM Ded1 also have increased RE at 500 nM Ded1 (compare red lines in cols. 1-
298 2), which for certain mRNAs is of greater magnitude at 500 nM (relatively darker red bars in col.
299 2). The decrease in RE observed for a smaller number of mRNAs upon Ded1 addition (Fig. 2G,
300 blue lines) generally appears to be greater at 500 nM versus 100 nM Ded1 (cf. blue lines in cols.
301 1-2), which is also consistent with the results in Figs. 2E and F.
302 Examining the distributions of all mRNAs across 10 bins of increasing RE values at each
303 concentration of Ded1 revealed an obvious shift of mRNAs from bins of lowest RE to bins of
304 higher RE when Ded1 was included in the Rec-Seq reactions (Fig. 2H, cf. orange vs. blue and
305 magenta bars, particularly in the first three bins on the left). The similar distributions observed
306 for the 100 nM and 500 nM Ded1 data are consistent with results in Figs. 2F-G indicating that
307 stimulation by Ded1 is nearly saturated at 100 nM. These data suggest that Ded1 confers
308 relatively greater stimulation for mRNAs that are recruited by 43S PICs poorly in the absence of
309 Ded1. Supporting this conclusion, the increase in RE between reactions with 500 nM vs. no
310 Ded1 was greatest for the subset of mRNAs of lowest RE and least for the mRNAs with highest
311 RE in reactions without Ded1 (Fig. 2I). This finding recapitulates and extends previous results on
312 several individual mRNAs wherein Ded1 strongly stimulated 43S PIC recruitment of Ded1
313 hyper-dependent transcripts exhibiting poor recruitment in reactions lacking Ded1, while more

314 weakly stimulating Ded1 hypo-dependent mRNAs that could be recruited efficiently without
315 Ded1 (Gupta et al. 2018).
316 In summary, the Rec-Seq results are highly consistent among biological replicates and
317 reproducibly identify a subset of ~1000 of the 3052 mRNAs detected in the analysis for which
318 assembly of 48S PICs is strongly stimulated by Ded1, with a marked tendency for greater
319 stimulation for mRNAs that recruit PICs poorly in Ded1's absence. These data support previous
320 conclusions from in vivo ribosome profiling analysis of a *ded1-cs* mutant that a significant
321 number (~600 to ~1100) of yeast mRNAs exhibit heightened dependence on Ded1 relative to the
322 average mRNA (Ded1-hyperdependent transcripts) (Sen et al. 2015; Sen et al. 2019). The
323 previous ribosome profiling studies also identified transcripts exhibiting increased relative TEs
324 in *ded1* mutant cells deficient in Ded1 activity (Ded1-hypodependent transcripts), consistent with
325 translational repression by wild-type Ded1. It was unclear, however, whether the translational
326 efficiencies of these last mRNAs were truly elevated in *ded1* cells or merely reduced by a
327 smaller amount than the average transcript to yield an increase in relative TE. Owing to the
328 spike-in normalization employed here, it is clear that the absolute occupancies of 48S PICs at
329 mAUGs on mRNAs showing reduced REs on Ded1 addition are indeed diminished by Ded1,
330 although it remains unclear whether the repression is direct or results indirectly from increased
331 competition for limiting PICs conferred by enhanced PIC recruitment on the Ded1-stimulated
332 mRNAs. We examine this question further below.
333
334 **Transcripts showing strong Ded1 stimulation of 48S PIC assembly in Rec-Seq have long**
335 **and structured 5'UTRs.** The mRNAs judged to be hyper-dependent on Ded1 from Ribo-Seq
336 experiments on *ded1* mutants are enriched for transcripts with longer than average 5'UTRs with

337 a heightened propensity for forming secondary structures (Sen et al. 2015). To examine these
338 trends in our in vitro system, we divided the subset of all transcripts analyzed by Rec-Seq with
339 annotated lengths for their predominant 5'UTRs (N = 2804, (Pelechano et al. 2013)) into six bins
340 of equal size and plotted their average REs in the presence or absence of Ded1. In the absence of
341 Ded1, the average RE values for these bins is roughly constant for the first four 5'UTR length
342 bins and then decreases markedly in the fifth and sixth bins (Fig. 3A, orange). The addition of
343 Ded1 differentially enhanced RE values depending on 5'UTR length, conferring the largest
344 increase for transcripts with the longest 5'UTRs (bin 6), smaller increases for bins 3-5 having the
345 next longest 5'UTRs, and little or no increase for the mRNAs in bins 1-2 with the shortest
346 5'UTRs (Fig. 3A, cyan & purple vs. orange). The 5'UTR length trends were confirmed by
347 plotting median RE changes conferred by 100 nM or 500 nM Ded1 versus no Ded1 for all six
348 bins (Fig. 3B-C) which showed little or no stimulation in bins 1-2 and progressively larger
349 increases in bins 3 to 6. Consistent with this, comparing 500 nm to 100 nm Ded1 (Fig. 3D)
350 revealed that the higher concentration of Ded1 actually reduced the median REs of the mRNAs
351 with shortest 5'UTRs in bins 1-2, while increasing it for the transcripts with longest 5'UTRs in
352 bins 5-6.

353 To examine the correlation between 5'UTR secondary structure and the effects of Ded1 on
354 RE values, we used a compilation of propensities for secondary structure in the yeast
355 transcriptome (Kertesz et al. 2010) in which each nucleotide in 3000 different yeast transcripts
356 was assigned a "parallel analysis of RNA structure" (PARS) score based on its susceptibility to
357 digestion with single- or double-stranded specific nucleases in yeast mRNA reannealed in vitro.
358 In this analysis a higher PARS score denotes a higher probability of double-stranded
359 conformation. We calculated various cumulative PARS scores for 5'UTRs, including the sum of

360 scores for (i) all 5'UTR nucleotides (Total PARS); (ii) the 30 nt surrounding the start codon
361 (Start30 PARS; for mRNAs with a 5'UTR ≥15 nt); (iii) the highest cumulative score in any 30 nt
362 window (Max30 PARS). For each sequence interval, the 1874 transcripts observed in Rec-Seq
363 with available PARS data were divided into 6 bins of increasing PARS scores and examined for
364 RE changes conferred by Ded1 in Rec-Seq.

365 The average REs of mRNAs binned according to the 5'UTR Max30 PARS scores decline
366 steadily with increasing PARS scores in Rec-Seq reactions lacking Ded1 (Fig. 3E, orange).
367 Importantly, the negative effect of increasing Max30 PARS scores was essentially eliminated by
368 addition of 100 nM or 500 nM Ded1 (Fig. 3E, purple and cyan). Consistent with this, addition of
369 100 nM or 500 nM Ded1 confers significant increases in median RE that get progressively larger
370 with increasing Max30 PARS scores (Fig. 3F,G). Increasing Ded1 from 100 to 500 nM modestly
371 increased the median RE for mRNAs in the two highest Max30 PARS score bins (Fig. 3H).
372 Similar effects on average RE values were observed for 5'UTR Total PARS and Start30 PARS
373 scores (Fig. 3S-1A-D), with relatively greater Ded1 stimulation for the mRNAs with larger
374 scores for both parameters (Fig. 3-S1C-D). Coding sequence (CDS) length also correlated with
375 diminished average RE values (Fig. 3I), and this effect was reversed by Ded1 for the mRNAs
376 with longest CDS lengths in the last two or three bins at both 100 and 500 nM Ded1 (Fig. 3I-L).
377 We do not know why the average RE versus CDS length curves are U shaped in the presence of
378 Ded1 (Fig. 3I, green and purple lines). The correlation between Ded1 stimulation of RE and CDS
379 length could be indirect because CDS length also correlates with 5'UTR length such that
380 mRNAs with longer CDSs also tend to have longer 5'UTRs (Fig. 3-S1-E,F). Importantly,
381 correlations between Ded1 stimulation and 5' UTR lengths are evident for all three groups of
382 mRNAs containing distinct ranges of CDS lengths (Fig. 3-S2A-C). In contrast, a marked

383 correlation between Ded1 stimulation and CDS length was detected only for the group of
384 mRNAs with longest 5'UTRs (Fig. 3-S2D-F), and only the latter group showed a clear
385 correlation between 5'UTR length and CDS length (Fig. 3-S2G-I). Thus, the correlation between
386 Ded1 stimulation and CDS length appears to be indirect, driven by the tendency for the mRNAs
387 with the longest 5'UTRs to also have correspondingly longer CDSs. Overall, the Rec-Seq results
388 suggest that Ded1 efficiently overcomes the impediment to 48S PIC assembly posed by
389 structures within 5'UTRs, which are cumulative in longer 5'UTRs. This agrees with the
390 conclusion reached from Ribo-Seq analysis of *ded1* mutants in which Ded1-hyperdependent
391 mRNAs were found to have significantly higher median PARS scores for all 5'UTR intervals
392 tested as well as longer than average 5'UTR lengths (Sen et al. 2015).
393 We next examined the dependence of Ded1 enhancement of 48S PIC assembly on the
394 sequences surrounding the start codon. The context scores of AUGs, AUG_{CAI}, quantify the
395 similarity between the -6 to +3 positions surrounding a given AUG to the start codons of the 2%
396 most highly translated yeast mRNAs (Zur and Tuller 2013). These context scores range from
397 ~0.16 (poorest) to ~0.97 (best) among all yeast mAUG codons. Binning mRNAs by context
398 score reveals a steady increase in RE with increasing context scores in Rec-Seq reactions lacking
399 Ded1 (Fig. 3-S3A, orange), indicating that good sequence context around the AUG codon
400 promotes 48S PIC formation. However, inclusion of 100 or 500 nM Ded1 increases the average
401 and median RE values similarly for all bins of context scores (Fig. 3-S3A, cyan and purple; Fig.
402 3-S3B, C). We conclude that the stimulatory effects of Ded1 on 48S PIC formation are
403 independent of the sequence context surrounding the AUG codon. Thus, Ded1 preferentially
404 stimulates recruitment of mRNAs burdened with structured 5'UTRs but not with poor AUG
405 sequence context.

406

407 **Transcripts showing Ded1 stimulation of 48S PIC assembly in Rec-Seq include the**
408 **majority of Ded1-hyperdependent mRNAs identified by Ribo-Seq analysis of a *ded1***
409 **mutant.**

410 We next asked whether mRNAs exhibiting stimulation of 48S PIC assembly by Ded1 in
411 Rec-Seq include those judged to be hyper-dependent on Ded1 in vivo by Ribo-Seq analysis of
412 the *ded1-cs* mutant (Sen et al. 2015). First, to assess the similarity between the sets of mRNAs
413 examined in our Rec-Seq experiments and in previous Ribo-Seq experiments, we plotted RNA-
414 Seq reads for all mRNAs observed in Rec-Seq versus those from WT or *ded1-cs* yeast strains in
415 the Ribo-Seq experiments and found that they were very strongly linearly correlated with
416 Spearman coefficients (ρ) of 0.90 and 0.88, respectively (Fig. 4A, B). The mRNAs from the WT
417 and *ded1-cs* strains identified in Ribo-Seq experiments were also well correlated (ρ = 0.97) (Fig.
418 4C). Thus, despite having been prepared using somewhat different methods, the total mRNA
419 used in our Rec-Seq experiments was very similar in sequence abundance to that observed in
420 previous in vivo ribosome profiling experiments.

421 Importantly, we observed a highly significant correlation (ρ = 0.60, P = 4.2 x 10^{-300})
422 between the mRPFs from Rec-Seq reactions lacking Ded1 and 80S RPFs from Ribo-Seq
423 experiments with the *ded1-cs* mutant at the non-permissive temperature where Ded1 function is
424 impaired (Fig. 4D). We saw similar correlations between mRPFs from Rec-Seq reactions
425 containing 100 nM or 500 nM Ded1 and 80S RPFs from Ribo-Seq experiments on the WT
426 *DED1* strain (Figs. 4E-F; ρ = 0.53 and ρ = 0.54, respectively). A total of 3035 mRNAs were
427 detected in common across all these experiments. Thus, a marked correlation exists between the
428 amounts of translation on each mRNA observed in vivo (80S RPFs) measured in Ribo-Seq

429 experiments and 48S PIC formation measured in our in vitro Rec-Seq experiments, and this
430 holds at different levels of Ded1 activity.

431 We also observed significant correlations between ΔRE values measured in Rec-Seq for
432 reactions containing no Ded1 versus 100 nM or 500 nM Ded1 and changes in translational
433 efficiencies (ΔTE values) measured in Ribo-Seq for *ded1-cs* versus WT *DED1* cells at the non-
434 permissive temperature (Fig. 4G, H). Consistent with this, the mRNAs exhibiting increased REs
435 on addition of either concentration of Ded1 and the mRNAs showing decreased TEs in *ded1-cs*
436 versus *DED1* cells in Ribo-Seq all have significantly higher median 5'UTR lengths, Max30
437 PARS scores, or Total PARS scores compared to all observed mRNAs and to the mRNAs that
438 behave oppositely in Rec-Seq or Ribo-Seq (Fig. 4I-K). Strikingly, 80-90% of the mRNAs
439 showing significantly decreased TEs conferred by *ded1-cs* in Ribo-Seq displayed significantly
440 increased REs on addition of 100 nM or 500 nM Ded1 in Rec-Seq reactions (Fig. 4L, M).

441 Despite the significant correlations shown in Fig. 4A-H, it should be noted that 11% of
442 the Ded1-hyperdependent mRNAs showing TE reductions in *ded1-cs* cells in Ribo-Seq did not
443 exhibit significant stimulation of 48S PIC assembly by Ded1 in our Rec-Seq experiments (Fig.
444 4L, set of 39 mRNAs). Such mRNAs might be stimulated by Ded1 at a step following 48S PIC
445 assembly that is not monitored by Rec-Seq or they might require additional factors for Ded1
446 stimulation of 48S PIC assembly that are lacking in our Rec-Seq experiments. It is also evident
447 that the majority of mRNAs stimulated by 500 nM Ded1 in our Rec-Seq experiments were not
448 judged to be Ded1-hyperdependent in Ribo-Seq analysis of the *ded1-cs* mutant (Fig. 4L, set of
449 683 mRNAs; "Group Y"). This could be explained by the fact that TEs in the Ribo-Seq analysis
450 of the *ded1-cs* mutant were measured relative to the average transcript (Sen et al. 2015) and thus
451 both Ded1 hyper- and hypo-dependent transcripts could have decreased absolute translational

452 efficiencies in the Ded1-deficient mutant at the non-permissive temperature relative to WT cells,
453 but with the former decreased more than the average transcript and the latter decreased similar to
454 or less than the average. Consistent with this interpretation, bulk polysome assembly is
455 dramatically reduced only minutes after shifting the *ded1-cs* mutant to the non-permissive
456 temperature, indicating a reduction in translation initiation on a large fraction of mRNAs (Sen et
457 al. 2015). Because the Rec-Seq method employs an internal standard, the measured REs are
458 absolute rather than relative and thus lead to a larger set of mRNAs with increased RE upon
459 Ded1 addition than that for the relative TE reductions in the *ded1-cs* mutant at the non-
460 permissive temperature in the Ribo-Seq experiments. Consistent with this explanation, the 683
461 Group Y mRNAs that were significantly stimulated in Rec-Seq by 500 nM Ded1 but not
462 classified as Ded1-hyperdependent in Ribo-Seq, displayed a smaller, albeit still significant,
463 median increase in RE upon addition of 500 nM Ded1 than did the 319 mRNAs ("Group X")
464 that were classified as Ded1 hyper-dependent in the Ribo-Seq experiments (Fig. 4N). Moreover,
465 the Group Y mRNAs had an approximately 3-fold smaller median decrease in relative TE
466 between the *ded1-cs* mutant and WT cells than did the Ded1 hyper-dependent Group X mRNAs
467 (Fig. 4O). The median TE change of Group Y mRNAs was less than 2-fold and thus would not
468 have met the criteria used for significance in the Ribo-Seq experiments. Thus, normalization of
469 TE changes to the average mRNA in Ribo-Seq undoubtedly obscured the Ded1-dependence in
470 vivo of many of the mRNAs stimulated by Ded1 in Rec-Seq reactions.

471 Together, our findings suggest that despite the much greater complexity of the system in
472 vivo in terms of both components and processes, the effects of Ded1 on the translation of many
473 mRNAs in cells is similar to what we see in the reconstituted Rec-Seq system that contains only
474 a core set of translation components and is not influenced by processes such as mRNA transport,

475 decay and compartmentalization/phase separation. This seems a remarkable result given the
476 number of in vivo roles that have been ascribed to Ded1 beyond simply promoting mRNA
477 recruitment and scanning. The significant correlation between the effects of adding Ded1 to Rec-
478 Seq experiments in vitro and of inactivating Ded1 in Ribo-Seq in vivo leads to the important
479 insight that 48S PIC formation is frequently the rate limiting step for translation initiation that is
480 stimulated by Ded1 in vivo.
481
482 **Evidence that Ded1 can promote leaky scanning of canonical AUG start codons.**
483 In Rec-Seq reactions lacking Ded1, RPFs at internal AUG start codons (iAUGs) located
484 within CDSs (iRPFs) occur at 3.0% of all RPFs found anywhere in the CDS (at either the main
485 or internal start sites, cdsRPFs), but this proportion increases to 4.2% and 7.8% on addition of
486 100 or 500 nM Ded1 to the reactions (Fig. 5A). The increase in iRPFs as Ded1 concentration
487 increases is shown clearly by metagene plots for all transcripts (Fig. 5B-D) and for four specific
488 genes in Fig. 5E-H, three of which also illustrate that Ded1 can increase iRPFs at genes where
489 48S PIC assembly at the mAUG is not stimulated or is even reduced by Ded1 (Fig. 5E-G).
490 DESeq2 analysis reveals that Ded1 elicits >2-fold increases in iRPFs for 590 and 1586 mRNAs
491 at 100 or 500 nM Ded1, respectively, whereas only 1 or 2 transcripts showed reduced iRPFs on
492 addition of Ded1, out of all 3052 transcripts detected (Fig. 5I-J). Thus, induction of iRPFs by
493 Ded1 is widespread in Rec-Seq.
494 A hallmark of increased leaky scanning in an mRNA would be a reciprocal decrease in
495 mRPF when an increase in iRPF occurs (Fig. 5S-1A). This situation, particularly well-illustrated
496 for *ETT1* and *DBP5* in Fig. 5E-F, is consistent with Ded1-stimulated read-through of the mAUG
497 codon leading to PICs continuing to scan downstream and initiating at iAUGs instead.

498 Importantly, a reciprocal reduction in mRPFs and increase in iRPFs of comparable magnitude on
499 Ded1 addition is evident for the group of 182 mRNAs identified above (Fig. 2B) showing >2-
500 fold reduction of mRPFs at 500 nM Ded1 (Fig. 5K). Moreover, 125 (69%) of these 182
501 transcripts belong to the group of 1586 mRNAs identified in Fig. 5J displaying >2-fold increases
502 in iRPFs at 500 nM Ded1 (Fig. 5L, green/red intersection). These 125 transcripts are shown as
503 black dots in the scatterplot of changes in mRPFs at 500 nM vs. 0 nM Ded1 in Fig. 5M. To apply
504 a stringent criteria for leaky scanning, we identified the mRNAs among this last group of 125
505 mRNAs for which the increase in iRPFs is comparable in magnitude (>50%) to the decrease in
506 mRPFs in the manner expected if iRPFs arise from PICs that scan past the mAUG and initiate
507 internally instead (highlighted with yellow circles in Fig. 5M). An important outcome of this
508 analysis is that leaky scanning of the mAUG could account for at least 46% (84/182) of all
509 mRNAs showing decreased mRPFs on addition of 500 nM Ded1. Many of the remaining 56%
510 could arise from increased competition for 43S PICs caused by Ded1 stimulation of PIC
511 formation on other mRNAs with long, structured 5'UTRs, which are poorly recruited in the
512 absence of Ded1 but begin competing for PICs when Ded1 is added to the system.
513 Considering that Ded1 inhibits 48S PIC assembly at the mAUG codons of so few
514 mRNAs (only 182 out of 3052 tested), and that translation initiation continues on at least 46% of
515 these transcripts and merely shifts to iAUGs, our data do not support a model in which a high
516 concentration of Ded1 leads to widespread translational repression by causing mRNAs to
517 undergo phase-transitions into translationally silenced states. If this is a significant repressive
518 function of Ded1 in vivo, it likely requires even higher concentrations of Ded1, modification of
519 Ded1, or additional factors not present in the Rec-Seq system.

520 Among the 1586 transcripts showing significantly increased initiation at iAUGs at 500
521 nM Ded1, roughly ~1/3rd (508) exhibit increased rather than decreased mRPFs on Ded1 addition
522 (Fig. 5L, red/blue intersection). In fact, this trend is evident for the entire group of 1006 mRNAs
523 showing increased PIC assembly at the mAUGs at 500 nM Ded1 (Fig. 5N), although the median
524 increase in iRPFs conferred by 500 nM Ded1 (23.2 iRPFs) is smaller for this group than that
525 observed for the mRNAs described above where PIC assembly at the mAUG is repressed by
526 Ded1 (86 iRPFs, Fig. 5K). One possibility is that a high concentration of Ded1 increases
527 readthrough of mAUGs on a large fraction of mRNAs but that in most cases this low-level leaky
528 scanning is offset by larger increases in PIC attachment to mRNAs to yield a net increase in
529 mRPFs despite enhanced mAUG readthrough. Consistent with this proposal, box plots of RE
530 values show that the mRNAs with mRPFs increased by Ded1 are initiated inefficiently in the
531 absence of Ded1, whereas the mRNAs that display decreased mRPFs in the presence of Ded1
532 tend to be initiated very efficiently in Ded1's absence (Fig. 5S-1B). Presumably, because the
533 latter mRNAs do not exhibit significantly increased recruitment of 43S PICs when Ded1 is
534 added, the increased leaky scanning of their mAUGs induced by Ded1 is not offset by increased
535 overall recruitment of PICs, resulting in a net decrease in PIC assembly at the mAUGs.
536 To assess whether the sequence context around the mAUG influences its susceptibility to
537 Ded1-induced leaky scanning, we examined the average fraction of all coding sequence RPFs
538 (cdsRPF) that are iRPFs, a ratio we refer to as Relative Ribosome Occupancy ($RRO_{iRPF/cdsRPF}$), as
539 a function of the context score for the bases surrounding the mAUG. As shown in Fig. 5O, with
540 both 0 and 500 nM Ded1 the average $RRO_{iRPF/cdsRPF}$ decreases as the context scores around the
541 mAUGs increase (cyan and purple lines), consistent with the idea that the better the context the
542 more stably the PIC is bound and the less likely is leaky scanning through the mAUG. Plotting

543 the ratio of RRO values at 500 nM to 0 nM Ded1 yields a flat line with $\log_2\Delta$RRO values of
544 ~0.75 for all bins (Fig. 5O, orange line). These last results suggest that addition of 500 nM Ded1
545 increases the frequency of leaky scanning by ~1.7-fold regardless of mAUG context. This in
546 turn implies that Ded1 does not inspect the context sequence but rather promotes scanning to
547 reduce the dwell-time of the PIC at the AUG similarly for both weak and strong contexts.
548 Rather than invoking leaky scanning, it could be proposed that the RPFs formed at iAUGs
549 originate from a small fraction of mRNA isoforms with transcription initiation sites within the
550 CDSs (Arribere and Gilbert 2013; Lu and Lin 2019) that contain the internal initiation sites as
551 the first AUGs encountered on scanning from the cap. Alternatively, the iRPFs could be formed
552 on uncapped mRNAs cleaved at the 5' end in cells or in vitro, which would require cap-
553 independent initiation. In either case, Ded1 could stimulate PIC assembly at the iAUGs by the
554 same mechanism identified above for canonical mAUGs. Several lines of evidence argue against
555 this possibility and instead favor the Ded1-induced leaky scanning model proposed above. First,
556 the level of iAUG initiation relative to mAUG initiation (RRO) depends strongly on the
557 sequence context surrounding the mAUG (Fig. 5O), as expected for the leaky scanning model
558 but inconsistent with a model in which iAUG occupancy arises from 5'-truncated mRNA
559 isoforms or fragments. In addition, mRNAs that have a high level of iAUG occupancy relative to
560 mAUG occupancy (RRO $\geqslant$ 0.5) tend to have less secondary structure in the 5'-ends of their
561 coding sequences than do mRNAs with less iAUG occupancy (Fig. 5P, cols. 3-8, compare blue
562 and orange boxes), consistent with a model in which secondary structures just downstream of the
563 mAUG inhibit further scanning and diminish mAUG readthrough (Kozak 1990). This result is
564 not predicted by the truncated mRNA isoform/fragment model. Finally, it is difficult to account
565 for the reciprocal effects of Ded1 in repressing mRPFs while inducing iRPFs by comparable

566 amounts for the same genes (Fig. 5K) if the events occur independently on different transcript
567 isoforms.

568 Overall, these data suggest that a high Ded1 concentration increases leaky scanning of the
569 mAUG for approximately half (1586/3052; Fig. 5J) of the mRNAs in the yeast translatome that
570 were observed in this study. In some cases this leads to a decrease in mRPFs, and may account
571 for nearly 50% of the mRNAs for which Ded1 suppresses 48S PIC assembly at the mAUG,
572 while in others the overall enhancement of PIC loading on the mRNA induced by Ded1 likely
573 offsets the increased leaky scanning for a net stimulation of 48S PIC assembly at the mAUG.
574 The inhibitory effect of Ded1 on proper initiation at mAUGs for the subsets of mRNAs
575 described above for which mRPFs are significantly decreased by 500 nM Ded1 in the Rec-Seq
576 experiments also appears to be operative in vivo as the median TEs of these sets of mRNAs are
577 increased in *ded1-cs* cells at the non-permissive temperature relative to WT cells (Fig. 5-S2),
578 signifying Ded1-hypodependence. These data are consistent with Ded1 activity diminishing the
579 relative translation levels of these mRNAs in WT cells, in alignment with our observations in the
580 Rec-Seq experiments.

581

582 **Ded1 does not generally increase initiation at canonical AUG codons in Rec-Seq by**
583 **suppressing alternative initiation events in 5'UTRs.**

584 It has been proposed that a key function of Ded1 is to increase the fidelity of start codon
585 selection by promoting readthrough of upstream AUG (uAUG) and near-cognate codons to boost
586 the fraction of scanning PICs that initiate at the mAUG codon (Guenther et al. 2018). To
587 determine whether this mechanism operates in the reconstituted system, we analyzed the effect
588 of Ded1 in Rec-Seq reactions on the total RPFs mapping to the 5'-UTRs of mRNAs (uRPFs).

589 We observed that 40 – 60% of all uRPFs detected when Ded1 is present in the reaction mapped
590 to the *GCN4* 5'UTR (Fig. 6-S1), and we therefore excluded *GCN4* mRNA in calculating the
591 [total uRPF]/[total mRPF] ratio in order to measure effects on the overall translatome. In the
592 absence of Ded1, the ratio of total uRPFs to mRPFs was 0.0021 (Fig. 6A, col. 1). Addition of
593 100 nM Ded1 decreased the ratio to 0.0017 and increasing the concentration to 500 nM
594 decreased it further only slightly, to 0.0016 (Fig. 6A, cols. 2-3). These values are similar to the
595 0.0027 value measured for the ratio of uRPFs to mRPFs in WT yeast cells in a previous
596 ribosome profiling study of 5'UTR translation (Kulkarni et al. 2019), suggesting the level of
597 5'UTR translation occurring in the in vitro Rec-Seq system is within 2-fold of that taking place
598 in vivo. A decreased uRPF/mRPF ratio on addition of Ded1 is expected if Ded1 suppresses PIC
599 assembly at upstream start codons as proposed in the aforementioned model. However, even in
600 the absence of Ded1, uRPFs represent a very small fraction of all RPFs and this fraction is
601 decreased by only ~30% upon addition of Ded1.
602 We next visualized the effects of Ded1 on upstream initiation in individual mRNAs by
603 plotting the uRPFs in the absence of Ded1 vs. the presence of 100 or 500 nM Ded1 (Fig. 6B and
604 C, respectively). Going from 0 to 100 nM Ded1 led to a significant reduction (ΔRPFs < 0.5, FDR
605 < 0.05) in uRPFs for only 9 mRNAs (Fig. 6B, dark blue dots). Moreover, only one mRNA
606 (*SXM1*) showed a decrease in uRPFs comparable in magnitude (>50%) to the corresponding
607 increase in mRPFs in the manner expected if Ded1-stimulated leaky scanning of uAUGs
608 stimulates PIC assembly at the mAUG (Fig. 6B, yellow circle). In contrast, uRPFs for 14
609 mRNAs were significantly increased (ΔRPFs > 2, FDR < 0.05), presumably due to enhanced PIC
610 attachment to these mRNAs caused by addition of Ded1. Similar results were obtained in going
611 from 0 to 500 nM Ded1, which resulted in only 25 mRNAs with significantly decreased uRPFs,

612 and only two showing reductions >50% of the magnitude of the observed increase in mRPFs for
613 the mRNA (*MSC7* and *UIP5*), whereas 30 mRNAs showed significant increases in uRPFs (Fig.
614 6C). In addition, there are at least as many cases in which upstream initiation is increased rather
615 than decreased, most likely due to overall enhancement of PIC attachment to these mRNAs by
616 Ded1. These data indicate that under the conditions of the Rec-seq experiments, Ded1 directly
617 increases PIC attachment to mRNAs and scanning to the main start codons rather than primarily
618 functioning by diminishing inhibitory initiation in 5'UTRs.

619 Additional evidence supporting our conclusion came from comparing the magnitude of
620 changes in uRPFs versus mRPFs conferred by Ded1 for a group of 257 mRNAs containing RPFs
621 in both 5'UTRs and at mAUG codons exceeding a minimum threshold read abundance. Overall,
622 the mRPFs are an order of magnitude higher than uRPFs in the absence or presence of Ded1 at
623 either concentration (Fig. 6D, see median values below each column). Addition of 100 nM Ded1
624 decreases the median uRPFs by 2, from 10 to 8, but increases mRPFs by 80, from 65 to 145.
625 Likewise, with 500 nM Ded1 relative to no Ded1, uRPFs decrease by 4, whereas mRPFs
626 increase by 109. Thus, the magnitude of the RPF decreases in 5'UTRs are much too small to
627 account for the increases in RPFs at mAUG codons elicited by addition of Ded1. Taken together,
628 our data indicate that, at least in the reconstituted in vitro system, Ded1 functions by directly
629 increasing PIC attachment to mRNAs and scanning to the main start codons rather than by
630 diminishing inhibitory initiation in 5'UTRs.

631

632 **eIF4A plays a distinct role from Ded1 and stimulates recruitment of most mRNAs**
633 **regardless of their 5'UTR lengths or structures.**

634 Previous work in vitro and in vivo has indicated that eIF4A and Ded1 play distinct roles
635 in promoting translation initiation. In the reconstituted system, no assembly of 48S PICs was
636 observed for a variety of individual mRNAs in the absence of eIF4A but presence of Ded1,
637 indicating that Ded1 cannot take the place of eIF4A (Gupta et al. 2018). In contrast, 48S PIC
638 formation occurred efficiently on many mRNAs in vitro in the presence of eIF4A but absence of
639 Ded1, and all mRNAs studied required eIF4A for PIC assembly, regardless of their degree of
640 secondary structure (Pestova and Kolupaeva 2002; Yourik et al. 2017; Gupta et al. 2018). In vivo
641 ribosome profiling studies also led to the conclusion that eIF4A is universally required for
642 translation of most mRNAs, whereas Ded1 preferentially stimulates translation of mRNAs with
643 long, structured 5'UTRs (Sen et al. 2015).
644 Our results here strongly support the previous conclusions that Ded1 functions by
645 alleviating structural impediments to PIC loading and scanning in the 5'UTRs of particular
646 mRNAs burdened by these features. To probe further functional differences between Ded1 and
647 eIF4A, we performed Rec-Seq reactions in the absence of Ded1 and presence of either 5000 nM
648 (1X) or 500 nM (0.1X) eIF4A. It was not possible to do the experiment in the absence of eIF4A
649 because the factor is essential for 48S PIC formation on most, if not all, mRNAs. A scatterplot of
650 mRPFs at 5000 versus 500 nM eIF4A shows that PIC assembly at the mAUGs of most mRNAs
651 increases when the concentration of eIF4A is raised 10-fold (Fig. 7A, light blue density above
652 the diagonal). Of 2809 mRNAs observed in these experiments, 782 reached the level of
653 significance in DEseq2 analysis of $\geqslant$ 2-fold change in mRPFs and FDR < 0.05. Only one
654 mRNA (*SCW10*) met the criteria for significantly decreased mRPFs (Fig. 7A, dark blue dot).
655 Consistent with these results, increasing the eIF4A concentration from 500 to 5000 nM increased
656 the REs of almost all mRNAs, with a median change of ~5.7-fold (Fig. 7B, col. 1). By

657 comparison, addition of either 100 or 500 nM Ded1 in a background of 5000 nM eIF4A
658 increased the median RE by only 1.3-fold, with RE for many mRNAs not changing (Fig. 7B,
659 cols. 2-3). Rather, a large number of outliers are increased dramatically more than the median
660 ΔRE value when Ded1 is added to the reactions, consistent with the preferential stimulation of
661 48S PIC assembly by Ded1 for mRNAs with long, structured 5'UTRs shown above (Fig. 3). In
662 our previous Ribo-Seq experiments on an eIF4A mutant, where changes in TE were determined
663 relative to the effect on the average mRNA, the vast majority of mRNAs displayed no change in
664 relative TE despite a strong reduction in bulk translation, implying TE reductions of similar
665 magnitude for nearly all mRNAs (Sen et al. 2015).

666 To examine whether length or structure of 5'UTRs influences the stimulatory effects of
667 eIF4A in Rec-Seq, we plotted ΔRE values between 500 and 5000 nM eIF4A as a function of
668 5'UTR length or Max30 PARS values. Importantly, the median ΔRE values remain constant
669 across the first five bins of 5'UTR lengths and four bins of Max30 PARS scores and actually
670 decrease significantly in the sixth bins (Fig. 7C, D). This behavior contrasts with that described
671 above for addition of Ded1 to Rec-Seq reactions, which showed progressively greater
672 enhancement of RE as 5'UTR length and Max30 PARS scores increased (Fig. 3B, C, F and G).
673 The distinct effects of increasing eIF4A concentration versus addition of Ded1 on mRNAs
674 binned according to 5'UTR length, 5'UTR Max30 PARS, or 5'UTR Total PARS values are
675 depicted in Figs. 7E-G. Consistent with these results, inspection of RPF traces for individual
676 mRNAs reveals that eIF4A enhances 48S PIC assembly on mRNAs judged to be either hypo- or
677 hyper-dependent on Ded1 in Ribo-Seq experiments (Sen et al. 2015) (Fig. 7H-K). Overall, these
678 results are consistent with previous conclusions that eIF4A stimulates recruitment of all mRNAs,
679 regardless of their degree of secondary structure, whereas Ded1 specifically acts on mRNAs with

680 long, structured 5'UTRs. Our data are also in line with previous work indicating that Ded1 has
681 much stronger helicase activity than eIF4A (Rogers et al. 1999; Yang et al. 2007; Rajagopal et
682 al. 2012) and thus the former is likely to play a role in unwinding stable secondary structures
683 whereas the latter mediates engagement of mRNAs with the 43S PIC by resolving ensembles of
684 weaker interactions within mRNAs or by modulating the structure of the mRNA channel of the
685 40S ribosomal subunit (Sokabe and Fraser 2017; Yourik et al. 2017).
686

687 **DISCUSSION**

688 We have developed a deep sequencing-based approach, "Rec-Seq," for measuring the
689 efficiency with which 48S PICs form on each mRNA in the yeast transcriptome in a
690 reconstituted in vitro system. Using this approach, we have provided evidence that the DEAD-
691 box translation initiation factor Ded1 specifically stimulates 48S PIC formation on mRNAs with
692 long, structured 5'UTRs, which supports the model that the factor generally acts by unwinding
693 secondary structures in 5'UTRs to promote 43S PIC binding and scanning to locate the start
694 (Berthelot et al. 2004; Sen et al. 2015; Guenther et al. 2018; Gupta et al. 2018; Sen et al. 2019;
695 Sen et al. 2021). We showed that 48S PIC formation on a set of ~1000 mRNAs is significantly
696 less efficient in the absence of Ded1 than in its presence, demonstrating a positive function for
697 the factor on these mRNAs. It is striking that the Ded1-stimulated mRNAs identified in our in
698 vitro system include the great majority of mRNAs identified as being hyperdependent on Ded1
699 in vivo by ribosome profiling of a *ded1-cs* mutant. This concordance argues that the mRNAs
700 showing the strongest dependence on Ded1 for efficient translation in vivo are stimulated by the
701 factor at the stage of 48S PIC assembly. It further argues against the possibility that the TE
702 reductions observed for Ded1 hyperdependent mRNAs in *ded1-cs* cells frequently result from

703 dominant inhibitory properties of the mutant *ded1* proteins. Ded1 also stimulated 48S PIC
704 assembly in Rec-Seq for many mRNAs not classified as Ded1-hyperdependent by Ribo-Seq.
705 However, as explained above, translation of these mRNAs was likely impaired by the *ded1-cs*
706 mutation but to a degree that was less than the 2-fold cutoff required for statistical significance,
707 or that was less than the effect on the average mRNA and thus yielded a positive change in the
708 relative TE values determined in the Ribo-Seq analysis.

709 Previous studies have indicated that yeast Ded1 and its mammalian ortholog DDX3 can
710 stimulate the subunit joining step of translation initiation (Senissar et al. 2014; Wang et al. 2022).
711 Although our Rec-Seq system only montored steps up to 48S PIC formation and was not able to
712 probe effects on 60S subunit joining, it should be noted that nearly 90% of the Ded1-
713 hyperdependent mRNAs identified by Ribo-seq analysis of the *ded1-cs* mutant were also
714 identified in our in vitro Rec-Seq experiments monitoring only 48S PIC assembly. This result
715 argues strongly that Ded1 affects 48S PIC assembly both in vitro and in vivo, although it does
716 not rule out an additional effect of the factor on subunit joining.

717 Compared to the sizeable group of >1000 mRNAs for which 500 nM Ded1 stimulated 48S
718 PIC assembly, we identified a much smaller set of only 182 mRNAs for which 48S PIC
719 assembly was significantly repressed by Ded1 in Rec-Seq experiments. We obtained evidence
720 that at least 84 of these transcripts were repressed owing to Ded1-stimulated leaky scanning of
721 the mAUG codon rather than by Ded1 blocking PIC attachment or scanning. As a group, the
722 mRNAs exhibiting Ded1 repression in Rec-Seq show increased relative TE in Ribo-Seq analysis
723 of the *ded1-cs* mutant, regardless of whether they display evidence of Ded1-enhanced leaky
724 scanning of the mAUG codons in Rec-Seq (Fig. 5-S2). This behavior is consistent with loss of
725 Ded1 repression or with smaller than average reductions in TE in *ded1-cs* vs. WT cells. The

726 latter possibility is consistent with our finding that the 182 mRNAs inhibited by 500 nM Ded1 in
727 Rec-Seq assemble 48S PICs very efficiently without Ded1 (Fig. 5-S1). Being relatively
728 independent of Ded1 for PIC assembly, these mRNAs should experience a smaller than average
729 reduction in translation in *ded1-cs* cells owing to reduced competition for limiting 43S PICs with
730 the Ded1-dependent mRNAs that should be strongly impaired for PIC assembly. We argued
731 above that a similar mechanism can also explain the repression of RE by Ded1 in Rec-Seq
732 experiments for the subset of 98 mRNAs without evidence of appreciable leaky scanning of the
733 mAUG codon, owing to increased competition for 43S PICs with the Ded1-stimulated
734 transcripts. It remains to be seen whether Ded1 acts directly to repress 48S PIC assembly on any
735 individual mRNAs in yeast. It is possible that at higher concentrations of Ded1 than were
736 achievable in these in vitro experiments or in the presence of additional factors that modify
737 Ded1's ATPase or RNA binding activities the factor could directly inhibit a subset of mRNAs,
738 by acting as an mRNA clamp that impedes scanning by the PIC, or by sequestering the mRNAs
739 in insoluble condensates. It might be interesting in the future to test candidate factors in Rec-Seq
740 to determine if they switch Ded1 from being a stimulatory helicase to an inhibitory mRNA
741 clamp that removes transcripts from the soluble phase.
742 We found that the presence of 500 nM Ded1 in Rec-Seq reactions increased 48S PIC
743 assembly at internal AUG codons on ~50% of all detected transcripts. In ~1/3rd of these 1586
744 transcripts, there is a parallel increase in RPFs at the mAUG codons, suggesting that Ded1
745 stimulates 43S PIC attachment at the 5' ends of these transcripts to increase initiation
746 proportionately at all AUGs in the mRNA. As mentioned, in ~5% of the mRNAs (84/1586), the
747 increased internal initiation may result from leaky scanning of the mAUG codons, as we found a
748 comparable reduction in initiation at the mAUG. In this view, Ded1 might resolve secondary

749 structures positioned just downstream of the mAUG codon that increase the dwell-time of the
750 PIC and increase the probability of PIC assembly versus continued scanning downstream that
751 leads to initiation on iAUG codons, in the manner first described for mammals by Kozak (Kozak
752 1990). Interestingly, Ded1 enhanced this apparent mAUG read-through to similar extents
753 regardless of the mAUG context, which would imply that Ded1 promotes scanning of the PIC
754 past the mAUG without inspecting the context nucleotides surrounding it.

755 Ded1 also significantly reduced RPFs at upstream AUG and near-cognate start codons in the
756 5'UTRs of a small number of transcripts (25 mRNAs at 500 nM Ded1), possibly by the same
757 mechanism mentioned above involving unwinding of downstream secondary structures.
758 However, this reduction was associated with a comparable increase in RPFs at the mAUG for
759 only two of these mRNAs. Our findings that PIC assembly at uAUGs in the absence of Ded1 is
760 rare, and that suppression of these rare occurrences by Ded1 cannot explain the much larger
761 increases in initiation at the mAUGs conferred by Ded1, argue that, at least in this in vitro
762 system, Ded1 functions primarily by directly promoting 43S PIC attachment to mRNAs and
763 scanning to the main start codons rather than by diminishing inhibitory initiation in 5'UTRs.

764 Finally, our data show that Ded1 and eIF4A, another essential DEAD-box translation
765 initiation factor, have distinct functions. Unlike Ded1, which has pronounced specificity for
766 activating initiation on mRNAs with long, structured 5'UTRs, eIF4A strongly promotes
767 initiation on nearly all mRNAs, regardless of the length or degree of structure of their 5' leaders.
768 Because our system employs internal "spike-in" standards, we were able to measure the absolute
769 enhancement provided by eIF4A for mRNA recruitment upon increasing its concentration from
770 500 to 5000 nM, a 5.7-fold increase in median RE (Fig. 7B). In contrast, addition of Ded1 to the
771 system produced a much smaller change in median RE, of only 1.3-fold, while conferring much

772 larger effects, >10-fold, on many mRNAs with long, structured 5'-UTRs. These findings support
773 our previous conclusions from Ribo-Seq analysis of Ded1 and eIF4A mutants that Ded1
774 preferentially stimulates translation of mRNAs burdened with structured 5'UTRs while eIF4A
775 enhances the translation of nearly all mRNAs equally (Sen et al. 2015).

776 Our data provide information on the intrinsic efficiency of 48S PIC formation on cellular
777 mRNAs in the yeast translatome. In the presence of 500 nM Ded1, RE values follow a roughly
778 normal distribution spanning a 1000-fold range (Fig. 2H), indicating that even in the presence of
779 Ded1, there are still large differences in the intrinsic efficiencies with which mRNAs are
780 recruited to the 43S PIC and scanned to locate the start codon. In the presence of Ded1, there is
781 little dependence of RE on 5'UTR structure or length (Fig. 3A,E) and thus other mRNA
782 characteristics must set the 48S PIC formation efficiencies. The strength of sequence context
783 around the start codon has a modest (~2-fold) effect (Fig. 3S-2A), but not nearly enough to
784 explain the range of REs observed. The 1000-fold range we observe here is strikingly similar to
785 the range reported in a systematic study of 5'UTR variants in a yeast lysate-based translation
786 system (Niederer et al. 2022). In that work, the authors provided evidence that a variety of
787 sequence elements in 5'UTRs can enhance or inhibit translation initiation through a range of
788 mechanisms. Thus, it is likely that in the presence of Ded1, no single mRNA feature sets the
789 efficiency of 48S complex assembly and instead a multitude of effects and interactions are
790 involved, possibly including specific interactions between mRNA elements and initiation factors
791 or the ribosome (Niederer et al. 2022). In addition, mRNA elements outside of the 5'UTR,
792 including the poly(A) tail and its interaction with PABP, might influence the efficiency of 48S
793 PIC formation. Further studies will be required to elucidate fundamental principles and specific
794 cases of how mRNA sequences dictate translational efficiency.

795

796 **Study Limitations**

797 As with all studies, this one has caveats and limitations. The fidelity of start codon
798 recognition in the in vitro Rec-Seq system might differ from what occurs in vivo. Likewise, the
799 use of an unmodified, in vitro transcribed initiator tRNA might lead to altered patterns of start
800 codon recognition in the Rec-Seq system relative to what is observed within living cells.
801 Previous studies of start codon recognition in the in vitro reconstituted yeast translation initiation
802 system indicated that the general trend of start codon preference reflects what is expected from in
803 vivo studies, with AUG codons leading to the most stable PICs, followed by near-cognate
804 codons with first position mistmatches (Kolitz et al. 2009). The Rec-Seq system shows a very
805 strong preference for AUG codons over near-cognates (e.g., Figs. 1 and 6) and for good Kozak
806 consensus sequences surrounding the start codon (Fig. 5O). Nonetheless, it will be worthwhile in
807 future studies in the Rec-Seq system to explore the effects of buffer conditions, temperature and
808 tRNA modifications on start codon recognition fidelity and its interplay with initiation factors
809 and mRNA structure.

810 The current version of the Rec-Seq system isolates events up to and including formation
811 of a stable 48S PIC on an mRNA start codon, but does not allow these PICs to progress to 80S
812 initiation complexes via 60S subunit joining. It is possible that subunit joining and 80S complex
813 formation could alter some of the patterns we have observed here. For example, rapid subunit
814 joining could diminish the Ded1-induced leaky scanning we have observed by stabilizing the
815 complexes and making them resistant to displacement and further scanning. Further studies will
816 be required to assess this possibility as well as any potential effects of Ded1 on the subunit
817 joining step (Senissar et al. 2014; Wang et al. 2022). It should also be noted that the Rec-Seq

818 system does not disentangle the steps of PIC binding to mRNA, scanning, and start codon
819 recognition from one another and thus independent effects on each of these processes cannot
820 currently be assessed with the assay.

821 Finally, in these experiments we monitored endpoints for 48S PIC formation at a single
822 timepoint (15 min) under single-turnover conditions in which neither multiple rounds of
823 initiation on a single start codon nor ribosome reinitiation events would be observed. The use of
824 single timepoints rather than kinetic measurements likely obscured some time-dependent effects.
825 Future experiments in which multiple timepoints are taken might allow us to observe changes in
826 the kinetics of 48S PIC formation upon addition of Ded1 or other factors to the system. The fact
827 that we cannot observe multiple-turnover initiation or reinitiation events using this system could
828 limit its utility in studying translational control events that require these processes.

829

830 **MATERIALS AND METHODS**

831 **Purification of yeast total mRNA**

832 WT *Saccharomyces cerevisiae* strain F729/BY4741 (*MATa his3Δ1 leu2Δ0 met15Δ0*
833 *ura3Δ0)* (Winzeler et al. 1999) was cultured in Yeast Extract–Peptone–Dextrose (YPD) medium
834 to OD_{600} of ~1. Harvested cells were washed once with cold water and stored in -80°C before
835 use. The frozen cell pellet from a 500 ml culture was thawed on ice and mechanically disrupted
836 by vortexing with glass beads three times for 2 min each at maximum speed in a cold room (4°C)
837 in 2 ml of buffer RL (provided in the kit), 3 ml phenol:chloroform:isoamyl alcohol 25:24:1 (pH
838 5.2) and 3 ml ice cold glass beads. Following 5 min incubation at 65°C and 5 min centrifugation
839 at 14000 rpm in a Sorvall LYNX 6000 Superspeed centrifuge using a Fiberlite F14-14 x 50cy
840 rotor, the supernatant was transferred to a fresh tube and total RNA was prepared using a

841 GenElute total RNA purification Maxi kit (Sigma-Aldrich; RNB200) following the
842 manufacturer's protocol. 400 µg total RNA in 250 µl water was applied to a GeneElute mRNA
843 miniprep kit (Sigma-Aldrich; MRN70-1KT), following the manufacturer's protocol. The purified
844 total mRNA was treated by 5'-Phosphate-Dependent Exonuclease (Lucigen, TER51020) to
845 degrade RNAs with 5' monophosphates, such as 18S and 25S ribosomal RNAs, at 0.3 µg/µl
846 mRNA in 1X buffer A (provided in the kit), 1U/µl RiboGuard RNase Inhibitor (Lucigen;
847 RG90925), 0.1 U/µl 5'-Phosphate-Dependent Exonuclease. Following a 1 h incubation at 30°C,
848 the total mRNA was extracted using phenol:chloroform:isoamyl alcohol 25:24:1 (pH 5.2),
849 ethanol precipitated, resuspended in 10 mM Tris (pH 8.0) and stored in -80 °C. The mass
850 concentration of purified total mRNA was determined using the RNA concentration function on
851 a NanoDrop One (ThermoFisher). The mass concentration was then converted to a molar
852 concentration using an online tool "Weight to Molar Quantity (for nucleic acids) converter"
853 (https://www.bioline.com/media/calculator/01_07.html), using the average molecular weight of
854 nucleoside monophosphates and assuming the average length of mRNAs is 1,000 nt (Miura et al.
855 2008). 75% of mRNAs (2719 of 3640) not observed in the Rec-Seq analysis had densities below
856 the median (2.3 reads per nucleotide).
857
858 **Purification of 40S ribosome subunits and translation initiation factors**
859 Eukaryotic initiation factors eIF1, eIF1A, eIF2, eIF3, eIF4A, eIF4B, eIF4G·4E and eIF5
860 were expressed and purified as described previously (Acker et al. 2007; Mitchell et al. 2010;
861 Rajagopal et al. 2012; Gupta et al. 2018). 40S ribosomal subunits were prepared as described in
862 Munoz et al. (2017). Ded1 protein (N-terminal His6-tag, pET22b vector) was purified as
863 described previously (Gupta et al. 2018).

864

865 **Preparation of spike-in mRNAs and charged initiator tRNA**

866 The templates for *in vitro* transcription of the 5' fragments of *FLUC* and *RLUC* genes
867 were amplified by PCR from plasmid FJZ1061 (Zhou et al. 2020) using primers T7-FLUC and
868 FLUC-R for *FLUC*, T7-RLUC and RLUC-R for *RLUC* (Table S1). The mRNAs and initiator
869 tRNA were transcribed by run-off transcription using T7 RNA polymerase and gel purified as
870 described previously (Acker et al. 2007; Mitchell et al. 2010). mRNAs were capped (m7GpppG)
871 using GTP and vaccinia virus capping enzyme (Mitchell et al. 2010). Initiator tRNA was
872 methionylated *in vitro* using methionine and *E. coli* methionyl-tRNA synthetase as previously
873 described (Walker and Fredrick 2008; Yourik et al. 2017).

874

875 **mRNA recruitment assays on spike-in mRNAs and total mRNA**

876 48S PICs were assembled on pre-mixed spike-in mRNAs (molar ratio FLUC/RLUC ~
877 1:10) as described previously (Mitchell et al. 2010; Yourik et al. 2017) in 1X Recon buffer (30
878 mM HEPES-KOH, pH 7.4, 100 mM KOAc, 3 mM Mg(OAc)2, and 2 mM DTT) containing 300
879 nM eIF2, 0.5 mM GDPNP·Mg^{2+}, 200 nM Met-$tRNA_i$Met, 1 μM eIF1, 1 μM eIF1A, 300 nM
880 eIF5, 300 nM eIF4B, 300 nM eIF3, 30 nM 40S subunits, 5 μM eIF4A, 30 nM eIF4E·eIFG, 5 μM
881 Ded1 and 15 nM mRNA. The reaction was incubated at 26°C for 20 min before being rapidly
882 quenched by adding stop buffer (1X Recon buffer, 37.5 mM glucose and 0.04 U/μl Hexokinase
883 (Roche Diagnostics, REF:11426362001)) in a 3:10 v/v ratio. RPFs of 48S PICs were generated
884 by incubating the reaction with RNase I (Thermo Fisher; AM2295) at a final concentration 2.5
885 U/μl, followed by adding SUPERaseIN RNase inhibitor (Thermo Fisher; AM2696) at a final
886 concentration 1.2 U/μl. Recruitment reactions using purified yeast total mRNA with different

887 Ded1 concentrations were performed similarly as for spike-in mRNAs, but incubated at 22°C for
888 15 min, with all of the same initiation factor concentrations except 60 nM input total mRNA and
889 three different Ded1 concentrations (0 nM, 100 nM and 500 nM), with 3 replicates for each
890 condition. The recruitment reactions were rapidly quenched by stop buffer and incubated with
891 RNase I to generate RPFs from 48S PICs as described above. Aliquots (4.5 µl) of spike-in RPFs
892 were mixed with the experimental sample RPFs and resolved on a 5-25% sucrose gradient by
893 ultracentrifugation for 3 h at 38,000 rpm and 4°C in an SW41Ti rotor in a Beckman Coulter
894 Optima XPN80 centrifuge. Fractions 6-13 of 20 total fractions were collected from the bottom of
895 each tube, extracted using phenol:chloroform:isoamyl alcohol 25:24:1 (pH 5.2), ethanol
896 precipitated, resuspended in 10 mM Tris (pH 8.0) and stored in -80 °C.
897
898 **Sequencing library construction**
899 RecSeq sequencing library construction was conducted according to a previously
900 described protocol (McGlincy and Ingolia 2017), with modifications, using identical barcoded
901 linkers (NI-810 to NI-815), RT primer (NI-802) and PCR primers (NI-798, NI-799, NI-822 to
902 NI-824). The RNA fragments purified from 48S PIC RPFs were dephosphorylated using T4
903 Polynucleotide Kinase (PNK) (NEB; M0201L) and ligated to pre-adenylated linkers (NI-810 to
904 NI-815) containing 5 nt sample barcodes unique for each sample using truncated T4 RNA ligase
905 2 (K227Q) (NEB; M0351L). Ligated fragments were separated from free linkers on a 15%
906 polyacrylamide TBE-Urea gel and then pooled and purified for reverse transcription using RT
907 primer NI-802 and ProtoScript II Reverse Transcriptase (NEB; M0368S). The ~105 nt cDNAs
908 were separated from free RT primers on a 15% TBE-Urea gel and circularized using
909 CircLigaseII ssDNA Ligase (Biosearch Technologies; CL9021K). PCR was carried out using

910 forward primer NI-798, and reverse primers (NI-799, NI-822 to 824) as already described
911 (McGlincy and Ingolia 2017) .
912 RNA-Seq for input total mRNA was performed as previously described (Ingolia et al.
913 2009; Ingolia 2010). Briefly, total mRNA was randomly fragmented at 70°C for 8 min in
914 fragmentation reagent (Thermo Fisher; AM8740) and size-selected for 50-90 nt fragments for
915 constructing a sequencing library using Universal miRNA Cloning Linker (NEB; S1315S) and
916 the RNA-Seq library construction procedures described above. Sequencing was done on an
917 Illumina NovaSeq 6000 system at the NHLBI DNA Sequencing and Genomics Core at NIH
918 (Bethesda, MD).
919
920 **Deep sequencing data processing and downstream analysis**
921 The constant linker sequence (AGATCGGAAGAGCAC) in barcoded linkers was
922 removed from Illumina NovaSeq reads using Cutadapt 4.0, and the mixed sample sequences
923 were separated by the sample barcodes and aligned to the *S. cerevisiae* non-coding RNA genome
924 using STAR 2.7.9a (Dobin et. al, 2013) to remove non-coding RNA reads. The remaining RNA
925 reads were then mapped to the reference genome (R64-1-1 S288C Sac cer3 Genome Assembly)
926 and spike-in "genome" using STAR 2.7.9a. Reads unaligned to the yeast genome were then
927 mapped to the spike-in genome to obtain spike-in RPF counts. Similarly, reads unaligned to the
928 spike-in genome were aligned to the yeast genome for genomic mRNA RPF counts. Size factors
929 for each sample were calculated using the geometric means of the numbers of 25-34 nt reads
930 mapping to both the mAUG and the many internal AUGs of the spike-in mRNAs, *FLUC* and
931 *RLUC*. Consistent with previous reports (Vandesompele et al. 2002), it was essential to use the
932 geometric mean rather than arithmetic mean for the spike-in normalizations, presumably because

933 of the exponential nature of the PCR amplification step of library construction. All samples were
934 normalized to the sample with highest spike-in geometric mean among 9 samples (3 replicates
935 each for 0 nm, 100 nm and 500 nm Ded1). Size-factor normalized wiggle tracks for each
936 replicate or average of replicates were produced from the alignment file, one each for genes on
937 the Watson or Crick strand. The sequences for the input total mRNA were processed similarly:
938 after trimming NEB universal linker sequences and removing non-coding RNAs, the remaining
939 reads were mapped to the yeast genome. Wiggle tracks were produced by assigning reads to the
940 position of their 5'ends. Two-dimensional metagene plots were produced by aligning all
941 genomic mRNAs to their mAUGs and plotting the density of all RPFs based on foot-print
942 lengths and the positions of their 5'ends map using a custom python script
943 (https://github.com/zhoufj/Metagene_plot).
944 For counting RPFs on mRNAs, all 25-34 nt Rec-Seq reads were assigned to their predicted
945 P-site mapped on the mRNA. The reads mapped between the -3 and +6 of the mAUG were
946 counted as main RPFs (mRPFs), the reads counted between the mAUG and the stop codon of the
947 CDS were counted as CDS RPFs (cdsRPFs), and the reads from the +9 position of the mAUG to
948 the stop codon counted as internal RPFs (iRPFs). mRNA read counts were determined for all
949 codons of the main CDS. DESeq2 (Love et al. 2014) was employed for differential expression
950 analysis of changes in RPF, recruitment efficiency (RE), or relative ribosome occupancy (RRO)
951 values, and to impose cutoffs for minimum read numbers (as indicated in figure legends) and
952 remove outliers. Size-factors calculated from spike-in RPFs were applied in DESeq2 analysis as
953 customized size-factors.
954
955 **Main AUG Context scores**

956 The AUG context adaptation index (context score) (Miyasaka 1999) for all mAUGs with
957 annotated 5'UTRs > 5 nt were previously calculated (Martin-Marcos et al. 2017).
958
959 **PARS scores**
960 The PARS scores, including Total, Max30, Start30, Plus15, Plus30 and Plus45 PARS were
961 caculated as previously described (Sen et al. 2015) using the same data set (Kertesz et al. 2010).
962 One caveat with our analyses using PARS scores is that we did not subject our mRNA
963 preparation to the final refolding protocol used by Kertesz et al. when they originally determined
964 the scores. It is possible that we would have seen stronger correlations in the analyses using
965 PARS scores had we followed their final renaturation protocol, although the fact that we
966 observed significant correlations (e.g., Fig. 3E-H) suggests the structures in the Kertesz et al.
967 mRNAs were similar to those in our mRNAs.
968
969 **Recruitment efficiency (RE) calculations**
970 Reads of input RNA-Seq were counted from the main start codon to the stop codon and
971 normalized to CDS length to calculate mRNA density. The recruitment efficiencies (REs) for
972 each mRNA in each codition were calculated as the ratio between the nomalized mRPF value
973 and mRNA density.

974 **ACCESSION NUMBER**

975 Sequencing data from this study have been submitted to the NCBI Gene Expression Omnibus
976 (GEO; http://www.ncbi.nlm.nih.gov/geo/) under the accession number GSE244093.
977

ACKNOWLEDGMENTS

This work was supported by the Intramural Research Program of the *Eunice Kennedy Shriver* National Institute of Child Health and Human Development. We thank other members of our laboratories and those of Tom Dever and Nick Guydosh for many helpful suggestions. We thank Ryan K Dale in NICHD/NIH Bioinformatics and Scientific Programming Core and Byung-sik Shin for their helps in sequencing data processing.

985 **Figure Legend:**

986 **Figure 1. Recruitment Sequencing (Rec-Seq) allows transcriptome-wide analysis of early**
987 **steps of translation initiation in a purified system.**

988 (**A**) Overview of steps in the Rec-Seq method. 48S ribosomal pre-initiation complexes (PICs)
989 are assembled in vitro from purified *S. cerevisiae* components. 48S PICs are treated with RNase
990 I to digest unprotected mRNA and then isolated using sucrose density gradient
991 ultracentrifugation. Ribosome-protected mRNA fragments (RPFs) are used to construct a
992 sequencing library. **(B-D)** Metagene plots of RPF distributions over 150 nt windows (-50 to +100
993 nt) on all mRNAs aligned to their main AUG start codons for no Ded1 (B); 100 nM Ded1 (C), or
994 500 nM Ded1 (D). RPF lengths are shown on the Y axis and the position of the 5'ends of the
995 RPFs relative to the main start codon are shown on the X axis. A 5'end located 12 nt from the
996 start codon is expected for 48S PICs with the AUG in the P site of the 40S subunit (Wagner et al.
997 2020). The color scale shows RPF density. All reads for 3 replicates for each condition were
998 combined. **(E, F)** RPFs for the 0, 100 and 500 nM Ded1 experiments for previously identified
999 Ded1 hypo-dependent (*OST3,* E) and hyper-dependent (*HOR7,* F) mRNAs. The position of the
1000 main CDS is shown in cyan and the −3 to −1 and +4 context nucleotides surrounding the main
1001 AUG are shown in brick red text. mRNA sequencing reads are also shown below each set of
1002 tracks (gray). The Integrated Genome Viewer (IGV, Broad Institute) was used to display RPF
1003 and mRNA reads, with RPF and nucleotide (nt) scales indicated on top of each panel. For these
1004 and all other gene browser views, the RPFs are plotted to their predicted P-site positions, and the
1005 mRNA reads are plotted to their first position from their transcript 5'ends.

1006

1007 **Figure 1-S1. A schematic diagram of mRNA recruitment in translation initiation.** The cap-
1008 binding protein complex eIF4F, consisting of eIF4E, eIF4G and eIF4A subunits attaches to the
1009 cap at the mRNA 5' end. The 43S PIC, which includes the 40S ribosomal subunit, eIFs 1, 1A, 3
1010 and 5 and the eIF2•GTP•Met-tRNA$_i$ ternary complex, binds to the 5' end of mRNA with the aid
1011 of the eIF4F complex and eIF4B and scans downstream in search of the start codon. A stable
1012 48S-PIC is formed when a start codon is recognized.
1013
1014 **Figure 1-S2. Internal spike-in normalization controls using preformed 48S PICs on non-**
1015 **native mRNAs**. **(A)** Steps in applying 48S-PIC spike-in controls for data normalization. Firefly
1016 and Renilla luciferase mRNAs (*FLUC* and *RLUC)* were in vitro transcribed from PCR-amplified
1017 gene templates containing T7 promoters and enzymatically capped using previously described
1018 protocols (Acker et al. 2007). The 48S PICs formed on the spike-in mRNAs were prepared
1019 separately from the testing samples in a recruitment reaction followed by RNase I treatment to
1020 digest unprotected mRNA. A constant amount of spike-in 48S PICs were resolved by
1021 sedimentation through the same sucrose gradients containing the experimental samples. The
1022 RPFs from these spike-in PICs served as internal controls for losses occurring during library
1023 construction and allowed data normalization across experimental samples. For deep sequencing
1024 data processing, non-coding RNA reads were removed and the remaining RPFs were aligned to
1025 spike-in mRNA sequences for calculating sample size factors and also aligned to the yeast
1026 genome to produce RPF counts on all yeast mRNAs. The RPF counts for all mRNAs in the
1027 genome were applied to DESeq2 using sample size factors calculated from the geometric means
1028 of spike-in mRNA RPFs mapped to *FLUC*/*RLUC* main AUGs and a number of internal AUGs.
1029 Recruitment efficiency (RE) values were calculated by normalizing the size-factor corrected

1030 RPFs to input mRNA densities. **(B-D)** Scatterplots of *FLUC* and *RLUC* RPF reads at the main
1031 and internal AUGs, in the first two of three replicate samples for each condition. The green
1032 diagonal line is for 1:1 ratio and the Spearman correlation coefficients (r) were calculated using
1033 "cor.test" function in R using option "method = spearman."
1034
1035 **Figure 1-S3. Transcriptome-wide reproducibility of RPFs among replicates**
1036 **(A-I)** Scatterplots of log2 main AUG ribosome occupancies (normalized by the geometric means
1037 of RPF reads on *FLUC* and *RLUC* spike-in mRNAs) for comparing each of two of the three
1038 replicates in different conditions, 0 nM Ded1 (A, D and G), 100 nM Ded1 (B, E and H) and 500
1039 nM Ded1 (C, F and I) for all mRNAs with ⩾ 90 total RPF reads in the 9 samples combined.
1040 Spearman correlation coefficients (r) were calculated as in Fig. 1-S2B-D.
1041
1042 **Figure 1-S4. RPFs on main AUGs are consistent among replicates.**
1043 **(A)** Box plot analysis of normalized RPF reads for 3052 mRNAs with > 90 total reads in 9
1044 samples (each of 3 replicates for 0, 100 and 500 nM Ded1). **(B-I)** 48S PIC-protected fragments
1045 (RPFs) and input mRNA reads for 3 replicates of each of the 3 conditions (0, 100 and 500 nM
1046 Ded1) on 8 example mRNAs across 3' portions of the 5'UTR and 5' portions of the CDS regions
1047 flanking the main AUGs. RPF and nt scales are shown in the top right corner of each panel. The
1048 position of the main CDS and the −3 to −1 and +4 context nucleotides surrounding the main
1049 AUG are labeled as in Fig. 1E-F. mRNAs shown are (B) *NPT1*; (C) *PMA1*; (D) *SFT2*; (E) *ICE2*;
1050 (F) *AIM41*; (G) *RCP10*; (H) *RPL41A;* and (I) *RPL16A*.
1051
1052 **Figure 2. Ded1 promotes the recruitment of a group of 1000 mRNAs.**

1053 **(A-C)** Scatterplots of normalized read densities on the main start codons of mRNAs (mRPF,
1054 number of RPFs mapping to the main AUG normalized by the geometric means of the spike-in
1055 internal control RPFs) for 3052 mRNAs with > 90 total reads in 9 samples (3 replicates each for
1056 0, 100 and 500 nM Ded1) for 100 versus 0 nM Ded1 (A), 500 versus 0 nM Ded1 (B), or 500
1057 versus 100 nM Ded1 (C). mRNAs with significantly changed recruitment were defined as those
1058 with false discovery rates (FDR) < 0.05 and RPF changes (ΔRPF) of > 2 for increased or < 0.5
1059 for decreased are indicated in red or dark blue, respectively. The number of significantly changed
1060 mRNAs are indicated in red (increased) and blue (decreased). (**D and E**) Overlaps between the
1061 mRNAs displaying significantly increased (D) or significantly reduced (E) mRPFs between 100
1062 and 500 nM Ded1 conditions. P-values for the overlap between each group were calculated using
1063 an online tool (http://nemates.org/MA/progs/overlap_stats.html). **(F)** Box plot analysis of the
1064 distribution and median of log2 change in mRPF between 0 and 100 nM Ded1 ($\Delta mRPF_{100/0\ nM}$
1065 $_{Ded1}$, orange) or 0 and 500 nM Ded1 ($\Delta mRPF_{500/0\ nM\ Ded1}$, cyan) for all 3052 mRNAs (cols. 1-2),
1066 and for the following 6 groups of mRNAs: 1006 or 911 for which mRPFs were significantly up
1067 in 500 or 100 nM Ded1, respectively, relative to no Ded1 (cols. 3-6, for red dots in B and A);
1068 793 mRNAs for which mRPFs were significantly up with both 100 and 500 nM Ded1 (cols. 7-8,
1069 for the overlapping mRNAs in D); 182 and 71 mRNAs for which mRPFs were significantly
1070 down in 500 or 100 nM Ded1 relative to no Ded1 (cols. 9-12, blue dots in B and A); and 48
1071 mRNAs for which mRPFs were significantly down with both 100 and 500 nM Ded1 (cols.13-14,
1072 for the overlaps in E). The blue horizontal line shows no change in mRPFs (ΔmRPF = 1). **(G)**
1073 Heat-map analysis of the recruitment efficiency changes $\Delta RE_{100/0\ nM\ Ded1}$, $\Delta RE_{500/0\ nM\ Ded1}$ and
1074 $\Delta RE_{500/100\ nM\ Ded1}$ for the 3052 mRNAs described in A-C, ordered by rank of $\Delta RE_{100/0\ nM\ Ded1}$
1075 from most increased (top) to most decreased (bottom) using the R heatmap.2 function. (**H**) The

1076 distributions of all observed mRNAs across 10 bins of increasing RE values at each
1077 concentration of Ded1 (0, 100, 500 nM). **(I)** Boxplot analysis of $\Delta RE_{500/0\ nM\ Ded1}$ for all 3052
1078 observed mRNAs binned by RE in the absence of Ded1 (RE_{-Ded1}) from the lowest to the highest.
1079

1080 **Figure 3. Ded1 promotes the recruitment of mRNAs with long or structured 5'UTRs.**
1081 **(A)** Line plot analysis of average recruitment efficiency (RE) for the 2804 mRNAs observed in
1082 the RecSeq experiments that have annotated 5'UTRs binned by 5'UTR length at 0, 100 and 500
1083 nM Ded1. Average RE values were determined from the RE values of all mRNAs in each bin.
1084 **(B-D)** Box plot analyses of the recruitment efficiency changes (ΔRE) between each of two
1085 different conditions for the same mRNA bins as in (A) for $\Delta RE_{100/0nM_Ded1}$ (B), $\Delta RE_{500/0nM_Ded1}$
1086 (C), or $\Delta RE_{500/100nM_Ded1}$ (D). **(E)** Line plot analysis of average RE values for the 1874 mRNAs
1087 observed in the RecSeq experiments with reported PARS scores binned according to Max30
1088 PARS scores from the lowest to highest. PARS scores were determined by Kertesz et al. (2010)
1089 and Max30 and other PARS score intervals were calculated as described in Sen et al. (2015). **(F-**
1090 **H)** Box plot analyses for the same mRNA bins as in (E) for $\Delta RE_{100/0nM_Ded1}$ (F), $\Delta RE_{500/0nM_Ded1}$
1091 (G), or $\Delta RE_{500/100nM_Ded1}$ (H). **(I)** Line plot analysis of average REs for all 3052 mRNAs divided
1092 into six equal-sized bins according to CDS lengths from the shortest to the longest for 0, 100 and
1093 500 nM Ded1. **(J-L)** Box plot analysis for the same mRNA bins as in (I) for $\Delta RE_{100/0nM_Ded1}$ (J),
1094 $\Delta RE_{500/0nM_Ded1}$ (K), or $\Delta RE_{500/100nM_Ded1}$ (L). All bins contain an equal number of mRNAs.
1095

1096 **Figure 3-S1. Ded1 preferentially stimulates 48S PIC formation on structured mRNAs. (A,**
1097 **B)** Line plot analysis of log2 average REs at 0, 100 and 500 nM Ded1for mRNAs binned
1098 according to total PARS scores (A) or the sum of PARS scores of the 30 nucleotides surrounding

1099 the start codon (for mRNAs with a 5'UTR of ⩾15 nt) (Start30 PARS, B). **(C, D)** Line plot
1100 analysis of log2 average ΔREs for 100/0 nM, 500/0 nM and 500/100 nM Ded1 for the 2035
1101 mRNAs observed in RecSeq that have annotated PARS scores binned according to Total PARS
1102 (C) or Start30 PARS (D) scores from the lowest to highest. **(E-F)** Box plots comparing 5'UTR
1103 or CDS lengths for the 4694 yeast mRNAs that have annotated 5'UTRs (Pelechano et al. 2013)
1104 for CDS lengths plotted for mRNAs binned by 5'UTR length from the shortest to the longest (E),
1105 or 5'UTR lengths plotted for mRNAs binned by CDS lengths from shortest to longest (F). All
1106 bins contain equal numbers of mRNAs.
1107
1108 **Figure 3-S2. Ded1 promotes the recruitment of mRNAs with long 5'UTRs independent of**
1109 **CDS lengths. (A-C)** Similar to Fig. 3C, but for mRNAs with different CDS length ranges, short
1110 (**A**, 78 – 804 nt, n=936), medium (**B**, 807-1389 nt, n=934) and long (**C**, 1392-7242 nt, n=934).
1111 **(D-F)** Similar to Fig. 3K, but for mRNAs with different 5'UTR length ranges, short (**D**, 1-31 nt,
1112 n=958), medium (**E**, 32-60 nt, n=925) and long (**C**, 1392-7242nt, n=921). **(G-I)** Box plot
1113 analysis of mRNA 5'UTR lengths for the same groups of mRNAs as in panels D-F, respectively.
1114
1115 **Figure 3-S3. Ded1 has little effect on discriminating main AUG context scores. (A)** Line plot
1116 analysis of average REs for the 2768 observed in RecSeq that have annotated 5'UTR lengths >5
1117 nt, divided into six equal-sized bins according to context scores from lowest to the highest at 0,
1118 100 and 500 nM Ded1. **(B-C)** Box-plot analyses of $\Delta RE_{100/0nM\ Ded1}$ (B) and $\Delta RE_{500/0nM\ Ded1}$ (C)
1119 values for the same mRNA bins as in (A).
1120

1121 **Figure 4. Ded1 dependencies observed in Rec-Seq experiments correlate strongly with in**
1122 **vivo results from previous ribosome profiling of the *ded1-cs* mutant.**
1123 **(A-B)** Scatterplots comparing Rec-Seq input RNA reads and ribosome profiling mRNA reads of
1124 WT (A) or *ded1-cs* (B) strains. (**C**) Scatterplot comparing ribosome profiling mRNA reads
1125 between WT and *ded1-cs* strains. **(D-F)** Scatterplots comparing 48S PIC RPFs from Rec-Seq to
1126 80S RPFs from ribosome profiling for the 3035 mRNAs that passed the significance cutoffs in
1127 both experiments for Rec-Seq at 0 nM Ded1 versus ribosome profiling of the *ded1-cs* mutant (D)
1128 or Rec-Seq at 100 nM (E) or 500 nM (F) Ded1 versus ribosome profiling of the WT strain. **(G-**
1129 **H)** Scatterplots comparing changes in translational efficiency (ΔTE) from ribosome profiling of
1130 the *ded1-cs* mutant versus WT to $\Delta RE_{0/100nM_Ded1}$ (G) or $\Delta RE_{0/500nM\ Ded1}$ (H) values from Rec-Seq.
1131 **(I-K)** Boxplot analysis of 5'UTR lengths (I), Max30 PARS (J), or Total PARS (K) for mRNAs
1132 with annotated 5'UTR lengths or PARS scores that showed significantly decreased (Down) or
1133 increased (Up) REs in 100 nM or 500 nM Ded1 versus no Ded1, or significantly increased (Up)
1134 or decreased (Down) TEs in the *ded1-cs* mutant versus WT. **(L-M)** Overlaps between mRNAs
1135 identified by Rec-Seq at 100 nM Ded1 (L) or 500 nM Ded1 (M) with significantly increased REs
1136 versus no Ded1 in Rec-Seq and mRNAs with significantly increased TEs in ribosome profiling
1137 of the *ded1-cs* mutant versus WT. P-values for the overlaps were calculated as described in Fig.
1138 2D-E**.** Group X and Y mRNAs in (L) are those in common between the two groups being
1139 compared (X) or those found exclusively in the set of 1002 mRNAs with significantly increased
1140 RE in 500 nM Ded1 versus no Ded1 in Rec-Seq (Y). **(N-O)** Boxplot analysis of log2
1141 $\Delta RE_{500/0nM_Ded1}$ (N) or log2 $\Delta TE_{ded1\text{-}ts\text{-}}$ (O) values for all 3035 mRNAs observed in both Rec-Seq
1142 and ribosome profiling, the 1002 mRNAs with significantly increased recruitment with 500 nM

1143 Ded1 versus no Ded1 (of L), the 319 mRNAs in group X (of L), and the 683 mRNAs in group Y
1144 (of L).
1145
1146 **Figure 5. Ded1 increases leaky scanning of main start codons**
1147 (**A**) The ratio of the total RPFs internal to the CDS in mRNAs, excluding the main start codon, to
1148 the total RPFs for the full CDS including the main start codon (iRPF/cdsRPF ratio) for each of
1149 the three replicates at 0, 100 and 500 nM Ded1. iRPFs were counted from the +9 position of the
1150 main AUG to the stop codon, while the cdsRPFs were counted from the start codon to the stop
1151 codon of the CDS. The average of the three replicates is indicated by the colored bars (red,
1152 green and blue for 0, 100 and 500 nM Ded1, respectively). **(B-D)** Metagene plots showing RPF
1153 density distribution on all mRNAs aligned to their main AUGs as in Fig. 1B-D for 0 (B), 100 (C)
1154 and 500 nM Ded1 (D), with color scales adjusted to show internal RPFs (iRPFs). **(E-H)** 48S PIC
1155 RPFs and input mRNA reads on four selected mRNAs that showed elevated internal ribosome
1156 occupancies in 100 and 500 nM Ded1 conditions. The -3 to -1 and +4 context nucleotides
1157 surrounding the main AUG, iAUG or upstream AUG (uAUG) are indicated in brick red text. **(I-**
1158 **J)** Scatterplots comparing log2 iRPF between 100 (I) or 500 nM Ded1 (J) to 0 nM Ded1 as
1159 described in Fig. 2A-B for the same group of 3052 mRNAs. Red dots show mRNAs that meet
1160 the significance cutoff for increases in iRPF (FDR < 0.05, >2-fold increase in iRPFs) and blue
1161 dots show mRNAs that meet the significance cutoff for decreases in iRPF (FDR < 0.05, <0.5-
1162 fold decrease in iRPFs). **(K)** Box plot comparing mRPFs and iRPFs between 500 and 0 nM
1163 Ded1 for the 182 mRNAs that showed significantly reduced mRPFs with 500 nM Ded1 versus
1164 no Ded1. **(L)** Overlaps between mRNAs with significantly elevated iRPFs (orange), significantly
1165 reduced mRPFs (green) or significantly increased mRPFs (blue) with 500 nM Ded1 relative to 0

1166 nM Ded1. The Venn diagram was generated and p-values calculated as in Fig. 2D. **(M)** Scatter
1167 plot comparing mRPFs with 500 nM versus 0 nM Ded1. The 125 mRNAs that showed
1168 significantly increased iRPFs and significantly decreased mRPFs in 500 nM Ded1 relative to 0
1169 nM Ded1 are labeled by black dots. Among this set, the mRNAs for which the iRPFs increase by
1170 at least 50% of the decrease in mRPFs are labeled by yellow circles, to indicate the 84 mRNAs
1171 for which the decrease in mRPFs could be responsible for the increase in iRPFs. **(N)** Boxplot
1172 comparing mRPFs and iRPFs between 500 nM and 0 nM Ded1 for the 1006 mRNAs that
1173 showed significantly increased mRPFs. **(O)** Line plot analysis of average RRO (relative
1174 ribosome occupancy; iRPF/cdsRPF ratio; left axis) and $\Delta RRO_{500/0\ nM\ Ded1}$ (right axis) for 2441 of
1175 3052 mRNAs in J with 5'UTR length >5 nt binned by main AUG context scores from lowest to
1176 highest. **(P)** Boxplot analysis of Start30, Plus15, Plus30 and Plus45 PARS scores for mRNAs
1177 with $RRO_{iRPF/cdsRPF} < 0.5$ (orange) or $\geqslant 0.5$ with 500 nM Ded1.

1178

1179 **Figure 5-S1. Supporting evidence that Ded1 promotes leaky scanning of the main start**
1180 **codon. (A)** Schematic of a 43S PIC leaky scanning through the main AUG and assembling at an
1181 internal AUG in the presence of Ded1. **(B)** Evidence that mRNAs whose recruitment is inhibited
1182 by 500 nM Ded1 in Rec-Seq assays generally assemble 48S PICs very efficiently without Ded1**.**
1183 Boxplot analysis of REs of groups of mRNAs at 0 nM (cyan) or 500 nM (yellow) Ded1 for all
1184 3052 mRNAs observed in Rec-Seq, the 1006 mRNAs with significantly increased mRPFs at 500
1185 nM Ded1 versus no Ded1 (Fig. 2B, red dots); and the 182 mRNAs with significantly decreased
1186 mRPFs with 500 nM Ded1 versus no Ded1 (Fig. 2B, blue dots).

1187

1188 **Figure 5-S2. mRNAs with reduced RE at 500 nM Ded1 versus no Ded1 in Rec-Seq assays**
1189 **tend to show increased relative TE in the *ded1-cs* mutant versus WT in ribosome profiling**
1190 **experiments.** Boxplot analysis of $\Delta TE_{ded1\text{-}cs}$ for the groups of mRNAs described in Figure 5L-M:
1191 The 182 mRNAs with mRPFs significantly reduced at 500 nM Ded1 versus no Ded1 (cyan); the
1192 125 mRNAs with significantly decreased mRPFs and increased iRPFs with 500 nM Ded1 versus
1193 no Ded1 (magenta); the 84 mRNAs from the previous set that had an increase in iRPFs that was
1194 at least 50% the of the decrease in mRPFs (yellow circles in Fig. 5M; orange).
1195
1196 **Figure 6. Ded1 modestly promotes readthrough of start codons in 5' UTRs of mRNAs.**
1197 **(A)** The ratios of RPFs in 5'UTRs to RPFs on main start codons (uRPF/mRPF ratios) for each of
1198 the three replicates with 0 (blue), 100 (magenta) or 500 (green) nM Ded1. The 5'UTR RPFs
1199 (uRPFs) were counted from the 5'end of the mRNA to the -5 position relative to the main AUG.
1200 The mean of the three replicates is indicated by the colored bars. uRPFs on *GCN4* mRNA were
1201 analyzed separately (Fig. 6-S1), because 42% and 57% of all uRPFs were mapped to the *GCN4*
1202 5'UTR in assays with 100 and 500 nM Ded1, respectively. **(B-C)** Scatterplots comparing uRPFs
1203 in the presence of either 100 nM (B) or 500 nM (C) Ded1 versus 0 nM Ded1. mRNAs with
1204 significantly increased or decreased uRPFs in the presence of Ded1 are indicated in red or dark
1205 blue dots, respectively. The criteria used for significance were FDR < 0.05 and a greater than 2-
1206 fold increase or decrease. Yellow circles denote the very few mRNAs whose uRPF read number
1207 decreases by more than 50% of the increases in their mRPF reads, indicating a clear reciprocal
1208 relationship between the decrease in uRPFs and the increase in mRPFs. (**D**) Box plot analysis of
1209 mRPF and uRPF read numbers for the 257 mRNAs that had both uRPFs and mRPFs ⩾ 2 reads

1210 averaged over all assays conducted at 0, 100 and 500 nM Ded1 concentrations. Unlogged median
1211 RPF numbers are labeled under each box.
1212
1213 **Figure 6-S1. Approximately half of all uRPFs map to the *GCN4* 5'UTR.** Percentages of all
1214 uRPFs mapped to the *GCN4* 5'UTR for each of the three replicates with 0 (blue), 100 (magenta),
1215 or 500 (green) nM Ded1 concentrations. Colored bars indicate the means of the replicates.
1216
1217 **Figure 7. eIF4A enhances the recruitment of almost all mRNAs**
1218 **(A)** Scatterplots of normalized read densities mapped to main AUGs (mRPFs) with 5000 nM
1219 versus 500 nM eIF4A for the 2809 mRNAs with ⩾ 8 total reads in 4 samples (2 replicates each
1220 for 5000 and 500 nM eIF4A). Red and blue dots show mRNAs with mRPFs significantly
1221 increased or decreased, respectively, at 5000 versus 500 nM eIF4A. The criteria for significance
1222 were FDR < 0.05 and a > 2-fold change in RPFs. **(B)** Boxplot comparing $\Delta RE_{5000/500\ nM\ eIF4A}$
1223 (grey) to $\Delta RE_{100/0\ nM\ Ded1}$ and $\Delta RE_{500/0\ nM\ Ded1}$ (cyan) for the 2698 mRNAs that passed the cutoff
1224 mentioned in (A) in both experiments. **(C)** Boxplot of $\Delta RE_{5000/500\ nM\ eIF4A}$ for the 2538 of all 2809
1225 mRNAs in (A) that have annotated 5'UTRs, divided into six equal sized bins according to
1226 5'UTR lengths from the shortest to the longest. (**D)** Similar to (C), but for the 1708 of all 2809
1227 mRNAs in (A) with annotated PARS scores, binned by Max30 PARS from lowest to highest. **(E-**
1228 **G)** Line plots of mean $\log_2$ RE changes, $\Delta RE_{5000/500\ nM\ eIF4A}$ (green), $\Delta RE_{100/0\ nM\ Ded1}$ (magenta),
1229 and $\Delta RE_{500/0\ nM\ Ded1}$ (blue), for mRNAs divided into six equal sized bins according to the specific
1230 mRNA features of 5'UTR length (E), Max30 PARS score (F), or Total PARS score (G). **(H-K)**
1231 RPFs assembled with 500 or 5000 nM eIF4A and input mRNA reads for mRNAs shown

1232 previously to be hypo-dependent on Ded1 (*RPC10*, *RPL41A*, *HOR7*) or hyper-dependent on

1233 Ded1(*PMA1*) by in vivo ribosome profiling experiments in the *ded1-cs* mutant.

1234

1235

REFERENCESUncategorized References

Acker MG, Kolitz SE, Mitchell SF, Nanda JS, Lorsch JR. 2007. Reconstitution of yeast translation initiation. *Methods Enzymol* **430**: 111-145.

Archer SK, Shirokikh NE, Beilharz TH, Preiss T. 2016. Dynamics of ribosome scanning and recycling revealed by translation complex profiling. *Nature* **535**: 570-574.

Arribere JA, Gilbert WV. 2013. Roles for transcript leaders in translation and mRNA decay revealed by transcript leader sequencing. *Genome Res* **23**: 977-987.

Beckham C, Hilliker A, Cziko AM, Noueiry A, Ramaswami M, Parker R. 2008. The DEAD-box RNA helicase Ded1p affects and accumulates in Saccharomyces cerevisiae P-bodies. *Mol Biol Cell* **19**: 984-993.

Berthelot K, Muldoon M, Rajkowitsch L, Hughes J, McCarthy JE. 2004. Dynamics and processivity of 40S ribosome scanning on mRNA in yeast. *Mol Microbiol* **51**: 987-1001.

Bresson S, Shchepachev V, Spanos C, Turowski TW, Rappsilber J, Tollervey D. 2020. Stress-Induced Translation Inhibition through Rapid Displacement of Scanning Initiation Factors. *Mol Cell* **80**: 470-484.e478.

Castelli LM, Lui J, Campbell SG, Rowe W, Zeef LA, Holmes LE, Hoyle NP, Bone J, Selley JN, Sims PF et al. 2011. Glucose depletion inhibits translation initiation via eIF4A loss and subsequent 48S preinitiation complex accumulation, while the pentose phosphate pathway is coordinately up-regulated. *Mol Biol Cell* **22**: 3379-3393.

Gao Z, Putnam AA, Bowers HA, Guenther UP, Ye X, Kindsfather A, Hilliker AK, Jankowsky E. 2016. Coupling between the DEAD-box RNA helicases Ded1p and eIF4A. *Elife* **5**.

Geissler R, Golbik RP, Behrens SE. 2012. The DEAD-box helicase DDX3 supports the assembly of functional 80S ribosomes. *Nucleic Acids Res* **40**: 4998-5011.

Guenther UP, Weinberg DE, Zubradt MM, Tedeschi FA, Stawicki BN, Zagore LL, Brar GA, Licatalosi DD, Bartel DP, Weissman JS et al. 2018. The helicase Ded1p controls use of near-cognate translation initiation codons in 5' UTRs. *Nature* **559**: 130-134.

Gulay S, Gupta N, Lorsch JR, Hinnebusch AG. 2020. Distinct interactions of eIF4A and eIF4E with RNA helicase Ded1 stimulate translation in vivo. *Elife* **9**.

Gupta N, Lorsch JR, Hinnebusch AG. 2018. Yeast Ded1 promotes 48S translation pre-initiation complex assembly in an mRNA-specific and eIF4F-dependent manner. *Elife* **7**.

Hilliker A, Gao Z, Jankowsky E, Parker R. 2011. The DEAD-box protein Ded1 modulates translation by the formation and resolution of an eIF4F-mRNA complex. *Mol Cell* **43**: 962-972.

Hinnebusch AG. 2014. The scanning mechanism of eukaryotic translation initiation. *Annu Rev Biochem* **83**: 779-812.

Hondele M, Sachdev R, Heinrich S, Wang J, Vallotton P, Fontoura BMA, Weis K. 2019. DEAD-box ATPases are global regulators of phase-separated organelles. *Nature* **573**: 144-148.

Ingolia NT, Ghaemmaghami S, Newman JR, Weissman JS. 2009. Genome-wide analysis in vivo of translation with nucleotide resolution using ribosome profiling. *Science* **324**: 218-223.

Iserman C, Desroches Altamirano C, Jegers C, Friedrich U, Zarin T, Fritsch AW, Mittasch M, Domingues A, Hersemann L, Jahnel M et al. 2020. Condensation of Ded1p Promotes a Translational Switch from Housekeeping to Stress Protein Production. *Cell* **181**: 818-831.e819.

1279 Kertesz M, Wan Y, Mazor E, Rinn JL, Nutter RC, Chang HY, Segal E. 2010. Genome-wide
1280 measurement of RNA secondary structure in yeast. *Nature* **467**: 103-107.
1281 Kolitz SE, Takacs JE, Lorsch JR. 2009. Kinetic and thermodynamic analysis of the role of start
1282 codon/anticodon base pairing during eukaryotic translation initiation. *Rna* **15**: 138-152.
1283 Kozak M. 1990. Downstream secondary structure facilitates recognition of initiator codons by
1284 eukaryotic ribosomes. *Proc Natl Acad Sci U S A* **87**: 8301-8305.
1285 Kulkarni SD, Zhou F, Sen ND, Zhang H, Hinnebusch AG, Lorsch JR. 2019. Temperature-
1286 dependent regulation of upstream open reading frame translation in S. cerevisiae. *BMC*
1287 *Biol* **17**: 101.
1288 Kumar P, Hellen CU, Pestova TV. 2016. Toward the mechanism of eIF4F-mediated ribosomal
1289 attachment to mammalian capped mRNAs. *Genes Dev* **30**: 1573-1588.
1290 Linder P, Jankowsky E. 2011. From unwinding to clamping - the DEAD box RNA helicase family.
1291 *Nat Rev Mol Cell Biol* **12**: 505-516.
1292 Love MI, Huber W, Anders S. 2014. Moderated estimation of fold change and dispersion for
1293 RNA-seq data with DESeq2. *Genome Biol* **15**: 550.
1294 Lu Z, Lin Z. 2019. Pervasive and dynamic transcription initiation in Saccharomyces cerevisiae.
1295 *Genome Res* **29**: 1198-1210.
1296 Martin-Marcos P, Zhou F, Karunasiri C, Zhang F, Dong J, Nanda J, Kulkarni SD, Sen ND, Tamame
1297 M, Zeschnigk M et al. 2017. eIF1A residues implicated in cancer stabilize translation
1298 preinitiation complexes and favor suboptimal initiation sites in yeast. *Elife* **6**.
1299 McGlincy NJ, Ingolia NT. 2017. Transcriptome-wide measurement of translation by ribosome
1300 profiling. *Methods* **126**: 112-129.
1301 Mitchell SF, Walker SE, Algire MA, Park EH, Hinnebusch AG, Lorsch JR. 2010. The 5'-7-
1302 methylguanosine cap on eukaryotic mRNAs serves both to stimulate canonical
1303 translation initiation and to block an alternative pathway. *Mol Cell* **39**: 950-962.
1304 Miura F, Kawaguchi N, Yoshida M, Uematsu C, Kito K, Sakaki Y, Ito T. 2008. Absolute
1305 quantification of the budding yeast transcriptome by means of competitive PCR
1306 between genomic and complementary DNAs. *BMC Genomics* **9**: 574.
1307 Miyasaka H. 1999. The positive relationship between codon usage bias and translation initiation
1308 AUG context in Saccharomyces cerevisiae. *Yeast* **15**: 633-637.
1309 Munoz AM, Yourik P, Rajagopal V, Nanda JS, Lorsch JR, Walker SE. 2017. Active yeast ribosome
1310 preparation using monolithic anion exchange chromatography. *RNA Biol* **14**: 188-196.
1311 Niederer RO, Rojas-Duran MF, Zinshteyn B, Gilbert WV. 2022. Direct analysis of ribosome
1312 targeting illuminates thousand-fold regulation of translation initiation. *Cell Systems* **13**:
1313 256-264.e253.
1314 Pelechano V, Wei W, Steinmetz LM. 2013. Extensive transcriptional heterogeneity revealed by
1315 isoform profiling. *Nature* **497**: 127-131.
1316 Pestova TV, Kolupaeva VG. 2002. The roles of individual eukaryotic translation initiation factors
1317 in ribosomal scanning and initiation codon selection. *Genes Dev* **16**: 2906-2922.
1318 Rajagopal V, Park EH, Hinnebusch AG, Lorsch JR. 2012. Specific domains in yeast translation
1319 initiation factor eIF4G strongly bias RNA unwinding activity of the eIF4F complex toward
1320 duplexes with 5'-overhangs. *J Biol Chem* **287**: 20301-20312.
1321 Rogers GW, Jr., Richter NJ, Merrick WC. 1999. Biochemical and kinetic characterization of the
1322 RNA helicase activity of eukaryotic initiation factor 4A. *J Biol Chem* **274**: 12236-12244.

1323 Schäfer T, Strauss D, Petfalski E, Tollervey D, Hurt E. 2003. The path from nucleolar 90S to
1324 cytoplasmic 40S pre-ribosomes. *Embo j* **22**: 1370-1380.
1325 Sen ND, Gupta N, S KA, Preiss T, Lorsch JR, Hinnebusch AG. 2019. Functional interplay between
1326 DEAD-box RNA helicases Ded1 and Dbp1 in preinitiation complex attachment and
1327 scanning on structured mRNAs in vivo. *Nucleic Acids Res* **47**: 8785-8806.
1328 Sen ND, Zhang H, Hinnebusch AG. 2021. Down-Regulation of Yeast Helicase Ded1 by Glucose
1329 Starvation or Heat-Shock Differentially Impairs Translation of Ded1-Dependent mRNAs.
1330 *Microorganisms* **9**.
1331 Sen ND, Zhou F, Ingolia NT, Hinnebusch AG. 2015. Genome-wide analysis of translational
1332 efficiency reveals distinct but overlapping functions of yeast DEAD-box RNA helicases
1333 Ded1 and eIF4A. *Genome Res* **25**: 1196-1205.
1334 Senissar M, Le Saux A, Belgareh-Touze N, Adam C, Banroques J, Tanner NK. 2014. The DEAD-box
1335 helicase Ded1 from yeast is an mRNP cap-associated protein that shuttles between the
1336 cytoplasm and nucleus. *Nucleic Acids Res* **42**: 10005-10022.
1337 Sokabe M, Fraser CS. 2017. A helicase-independent activity of eIF4A in promoting mRNA
1338 recruitment to the human ribosome. *Proc Natl Acad Sci U S A* **114**: 6304-6309.
1339 Sonenberg N, Hinnebusch AG. 2009. Regulation of Translation Initiation in Eukaryotes:
1340 Mechanisms and Biological Targets. *Cell* **136**: 731-745.
1341 Vandesompele J, De Preter K, Pattyn F, Poppe B, Van Roy N, De Paepe A, Speleman F. 2002.
1342 Accurate normalization of real-time quantitative RT-PCR data by geometric averaging of
1343 multiple internal control genes. *Genome Biol* **3**: Research0034.
1344 Wagner S, Herrmannová A, Hronová V, Gunišová S, Sen ND, Hannan RD, Hinnebusch AG,
1345 Shirokikh NE, Preiss T, Valášek LS. 2020. Selective Translation Complex Profiling Reveals
1346 Staged Initiation and Co-translational Assembly of Initiation Factor Complexes. *Mol Cell*
1347 **79**: 546-560.e547.
1348 Walker SE, Fredrick K. 2008. Preparation and evaluation of acylated tRNAs. *Methods* **44**: 81-86.
1349 Wang J, Shin BS, Alvarado C, Kim JR, Bohlen J, Dever TE, Puglisi JD. 2022. Rapid 40S scanning
1350 and its regulation by mRNA structure during eukaryotic translation initiation. *Cell* **185**:
1351 4474-4487.e4417.
1352 Winzeler EA, Shoemaker DD, Astromoff A, Liang H, Anderson K, Andre B, Bangham R, Benito R,
1353 Boeke JD, Bussey H et al. 1999. Functional characterization of the S. cerevisiae genome
1354 by gene deletion and parallel analysis. *Science* **285**: 901-906.
1355 Yang Q, Del Campo M, Lambowitz AM, Jankowsky E. 2007. DEAD-box proteins unwind duplexes
1356 by local strand separation. *Mol Cell* **28**: 253-263.
1357 Yourik P, Aitken CE, Zhou F, Gupta N, Hinnebusch AG, Lorsch JR. 2017. Yeast eIF4A enhances
1358 recruitment of mRNAs regardless of their structural complexity. *Elife* **6**.
1359 Zhou F, Zhang H, Kulkarni SD, Lorsch JR, Hinnebusch AG. 2020. eIF1 discriminates against
1360 suboptimal initiation sites to prevent excessive uORF translation genome-wide. *Rna* **26**:
1361 419-438.
1362 Zur H, Tuller T. 2013. New universal rules of eukaryotic translation initiation fidelity. *PLoS*
1363 *Comput Biol* **9**: e1003136.
1364

1365

1366

1367 Table S1: Oligonucleotides used for Spike-in mRNA template amplification

Primer name	**Sequence (5' – 3')**
T7-FLUC	AAGGAATTCATCTTAACTTT**TAATACGACTCACTATAG**GGCAAAC AAACAAACCAAAACCAAAACCACA***ATG***GAAGACGCCAAAAACATA
T7-RLUC	AAGGAATTCATCTTAACTTT**TAATACGACTCACTATAG**GGCAAAC AAACAAACCAAAACCAAAACCACC***ATG***ACTTGCAAAGTTTATGAT
FLUC-R	GTCGACGAGGAATTCATTATCAGTGC
RLUC-R	GTCGACTTCTCCTTCTTCAGATTTGATC

1368 Note: T7 promoter sequences are in boldface and underlined; mAUGs are in boldface and italicized

1369

1370

1371

1372

Figure 1

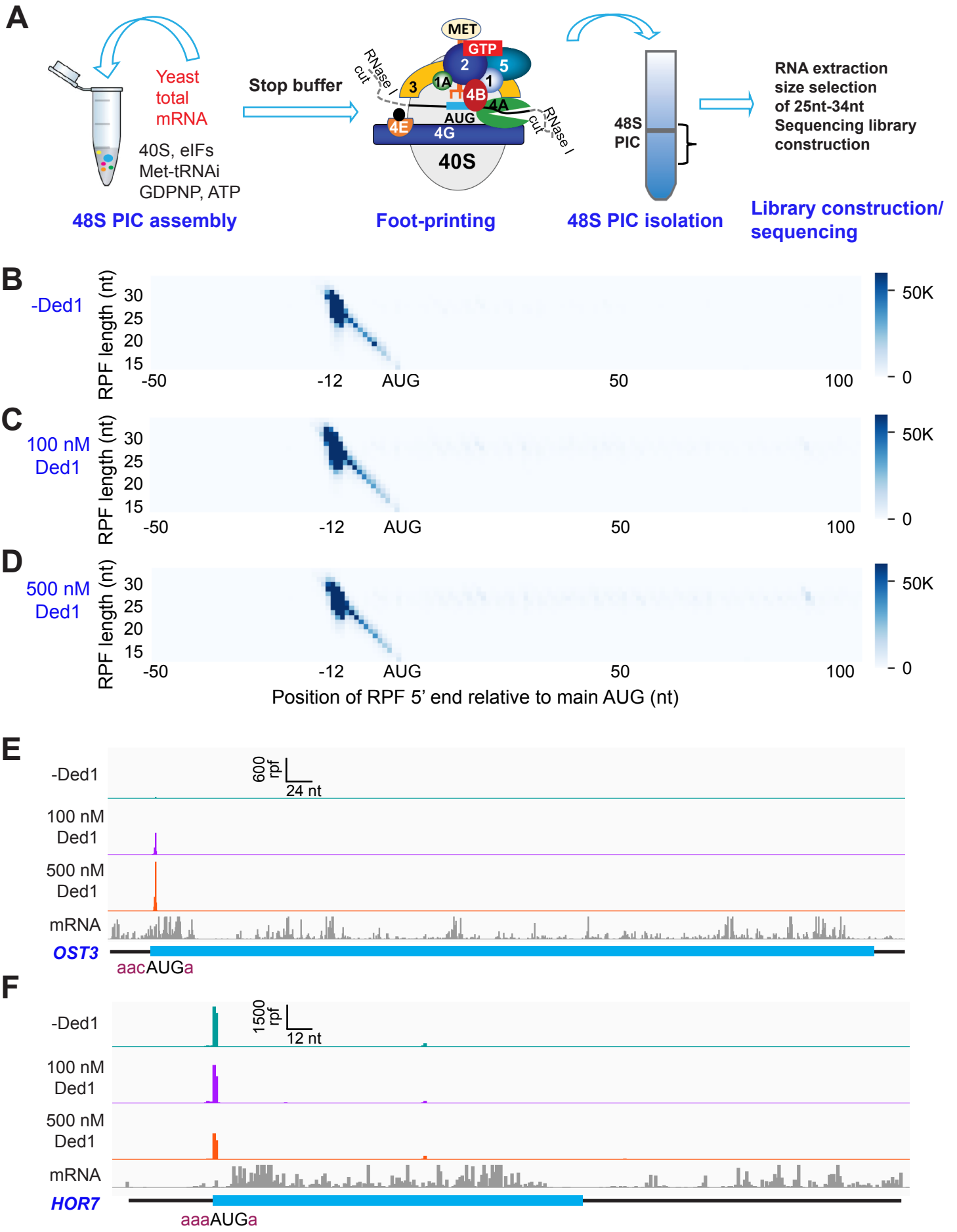
A
Yeast total mRNA
40S, eIFs
Met-tRNAi
GDPNP, ATP
48S PIC assembly
Stop buffer
MET
GTP
2
5
3
1A
1
4B
4A
AUG
4E
4G
40S
RNase I cut
RNase I cut
Foot-printing
48S PIC
48S PIC isolation
RNA extraction
size selection
of 25nt-34nt
Sequencing library
construction
Library construction/ sequencing
B
-Ded1
C
100 nM Ded1
D
500 nM Ded1
RPF length (nt)
30
25
20
15
-50
-12
AUG
50
100
50K
0
Position of RPF 5' end relative to main AUG (nt)
E
-Ded1
600 rpf
24 nt
100 nM Ded1
500 nM Ded1
mRNA
OST3
aacAUGa
F
-Ded1
1500 rpf
12 nt
100 nM Ded1
500 nM Ded1
mRNA
HOR7
aaaAUGa

Figure 1-S1

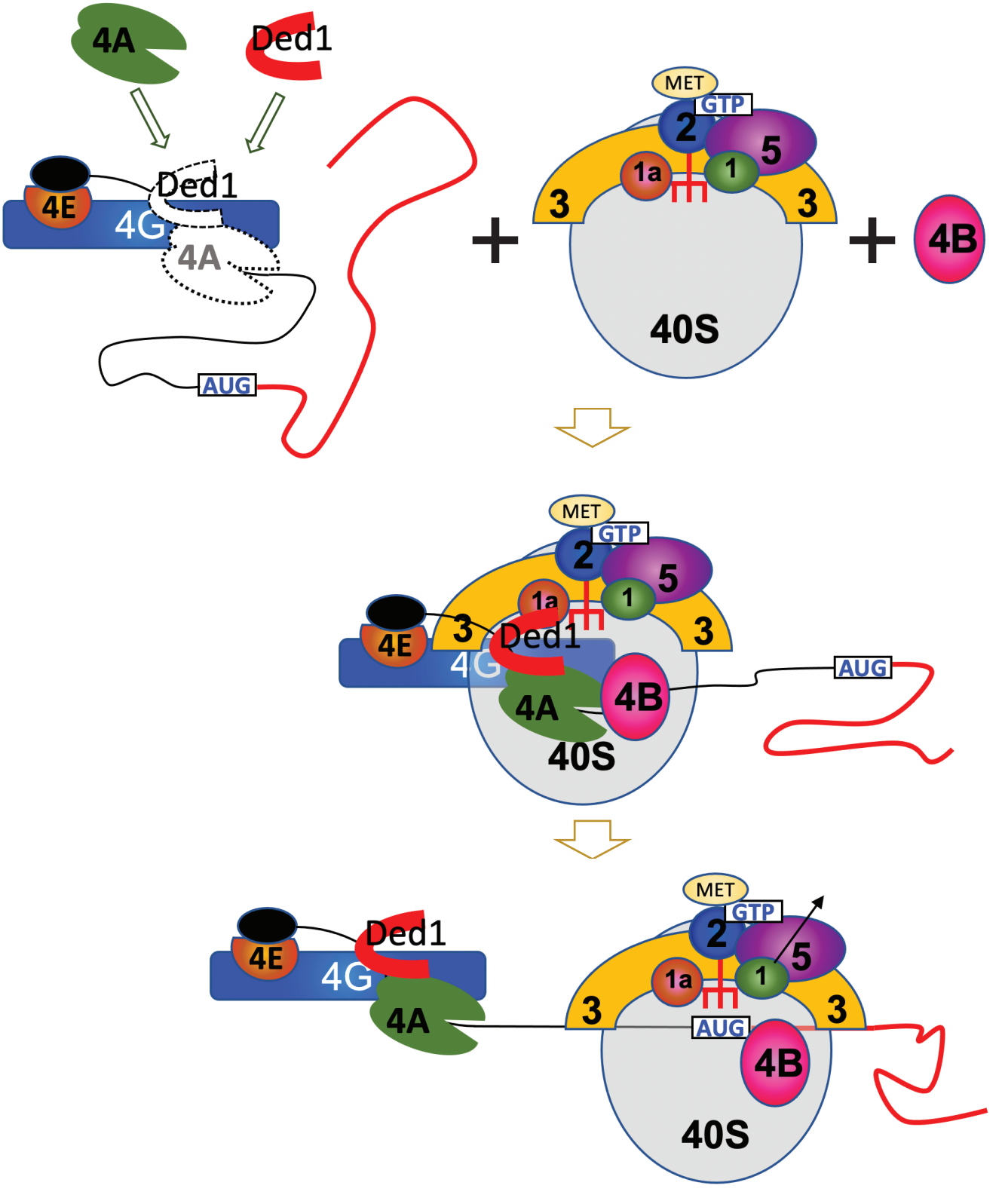
4A
Ded1
4E
4G
Ded1
4A
AUG
MET
GTP
2
5
1a
1
3
3
40S
4B
MET
GTP
2
5
1a
1
3
3
4E
Ded1
4G
4A
4B
AUG
40S
MET
GTP
2
5
1a
1
3
3
4E
Ded1
4G
4A
AUG
4B
40S

Figure 1-S2

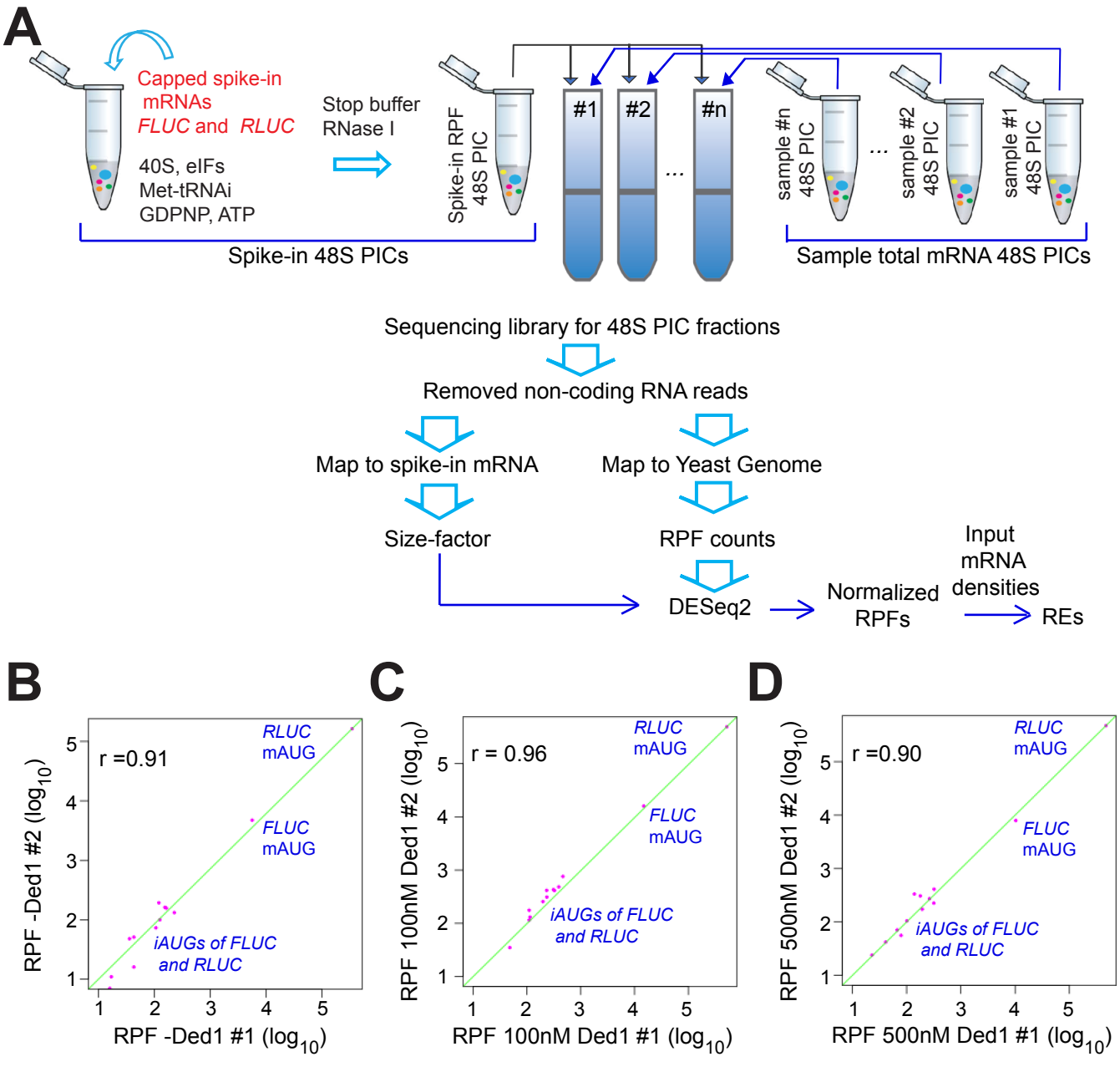
A
Capped spike-in mRNAs
FLUC and RLUC
40S, eIFs
Met-tRNAi
GDPNP, ATP
Stop buffer
RNase I
Spike-in RPF 48S PIC
#1
#2
#n
sample #n 48S PIC
sample #2 48S PIC
sample #1 48S PIC
Spike-in 48S PICs
Sample total mRNA 48S PICs
Sequencing library for 48S PIC fractions
Removed non-coding RNA reads
Map to spike-in mRNA
Map to Yeast Genome
Size-factor
RPF counts
DESeq2
Normalized RPFs
Input mRNA densities
REs
B
r =0.91
RLUC mAUG
FLUC mAUG
iAUGs of FLUC and RLUC
RPF -Ded1 #2 (log10)
RPF -Ded1 #1 (log10)
C
r = 0.96
RLUC mAUG
FLUC mAUG
iAUGs of FLUC and RLUC
RPF 100nM Ded1 #2 (log10)
RPF 100nM Ded1 #1 (log10)
D
r =0.90
RLUC mAUG
FLUC mAUG
iAUGs of FLUC and RLUC
RPF 500nM Ded1 #2 (log10)
RPF 500nM Ded1 #1 (log10)

Figure 1-S3

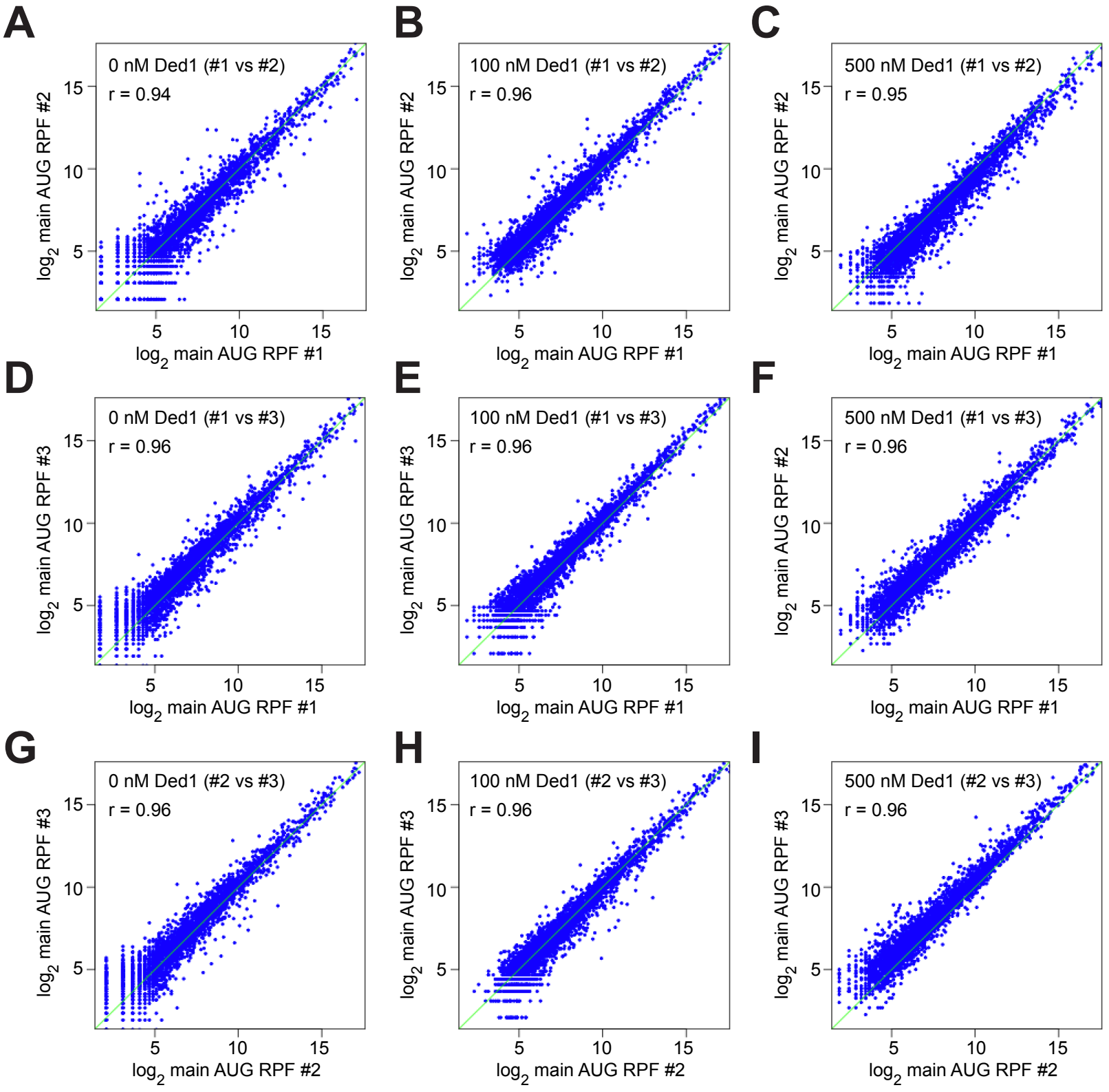
A
0 nM Ded1 (#1 vs #2)
r = 0.94
log2 main AUG RPF #2
log2 main AUG RPF #1
B
100 nM Ded1 (#1 vs #2)
r = 0.96
log2 main AUG RPF #2
log2 main AUG RPF #1
C
500 nM Ded1 (#1 vs #2)
r = 0.95
log2 main AUG RPF #2
log2 main AUG RPF #1
D
0 nM Ded1 (#1 vs #3)
r = 0.96
log2 main AUG RPF #3
log2 main AUG RPF #1
E
100 nM Ded1 (#1 vs #3)
r = 0.96
log2 main AUG RPF #3
log2 main AUG RPF #1
F
500 nM Ded1 (#1 vs #3)
r = 0.96
log2 main AUG RPF #2
log2 main AUG RPF #1
G
0 nM Ded1 (#2 vs #3)
r = 0.96
log2 main AUG RPF #3
log2 main AUG RPF #2
H
100 nM Ded1 (#2 vs #3)
r = 0.96
log2 main AUG RPF #3
log2 main AUG RPF #2
I
500 nM Ded1 (#2 vs #3)
r = 0.96
log2 main AUG RPF #3
log2 main AUG RPF #2

Figure 1-S4

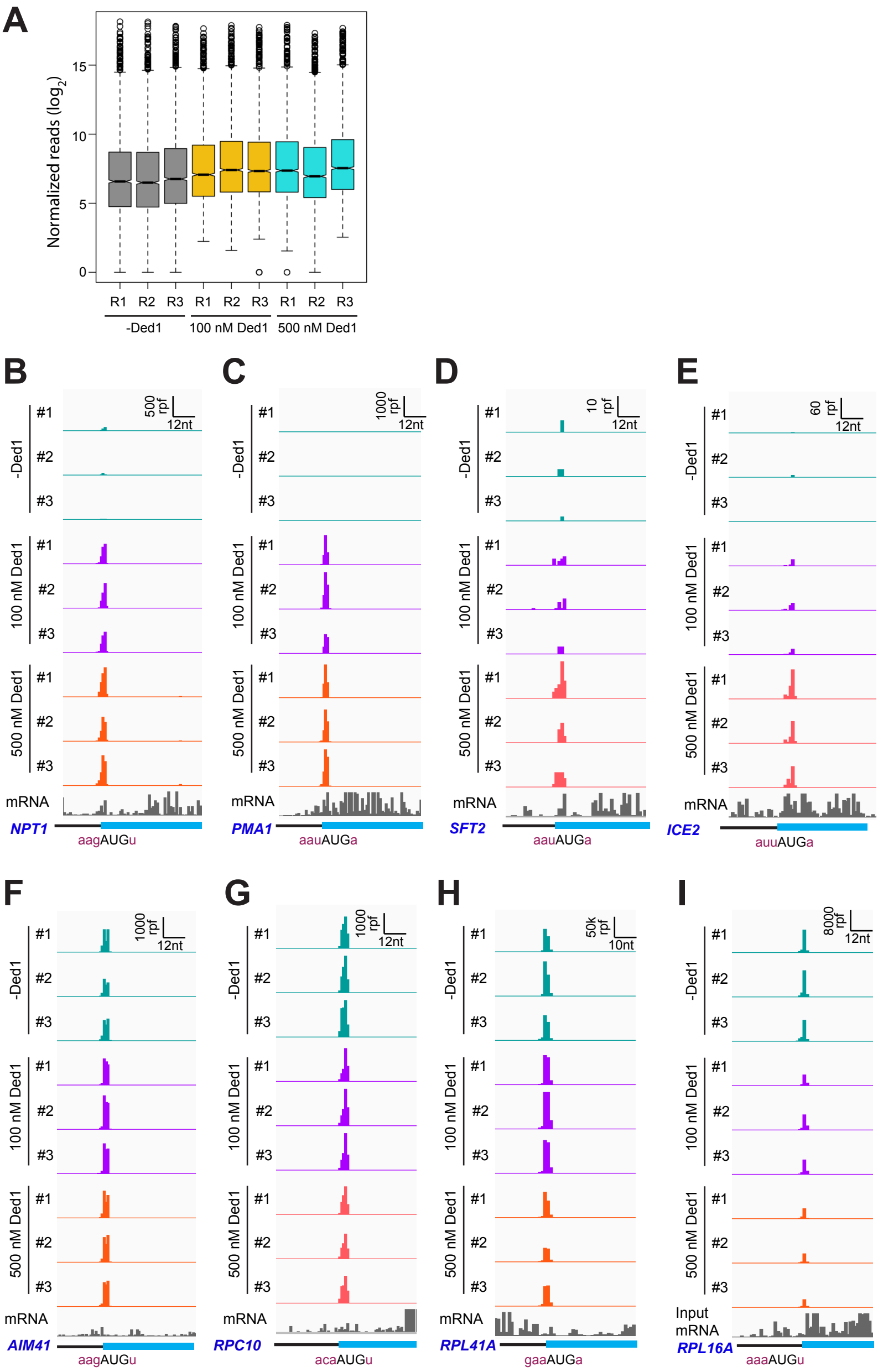
A
Normalized reads (log2)
15
10
5
0
R1 R2 R3 R1 R2 R3 R1 R2 R3
-Ded1
100 nM Ded1
500 nM Ded1
B
C
D
E
F
G
H
I
-Ded1
100 nM Ded1
500 nM Ded1
#1
#2
#3
500 rpf
1000 rpf
10 rpf
60 rpf
1000 rpf
1000 rpf
50k rpf
8000 rpf
12nt
10nt
mRNA
Input mRNA
NPT1
aagAUGu
PMA1
aauAUGa
SFT2
aauAUGa
ICE2
auuAUGa
AIM41
aagAUGu
RPC10
acaAUGu
RPL41A
gaaAUGa
RPL16A
aaaAUGu

Figure 2

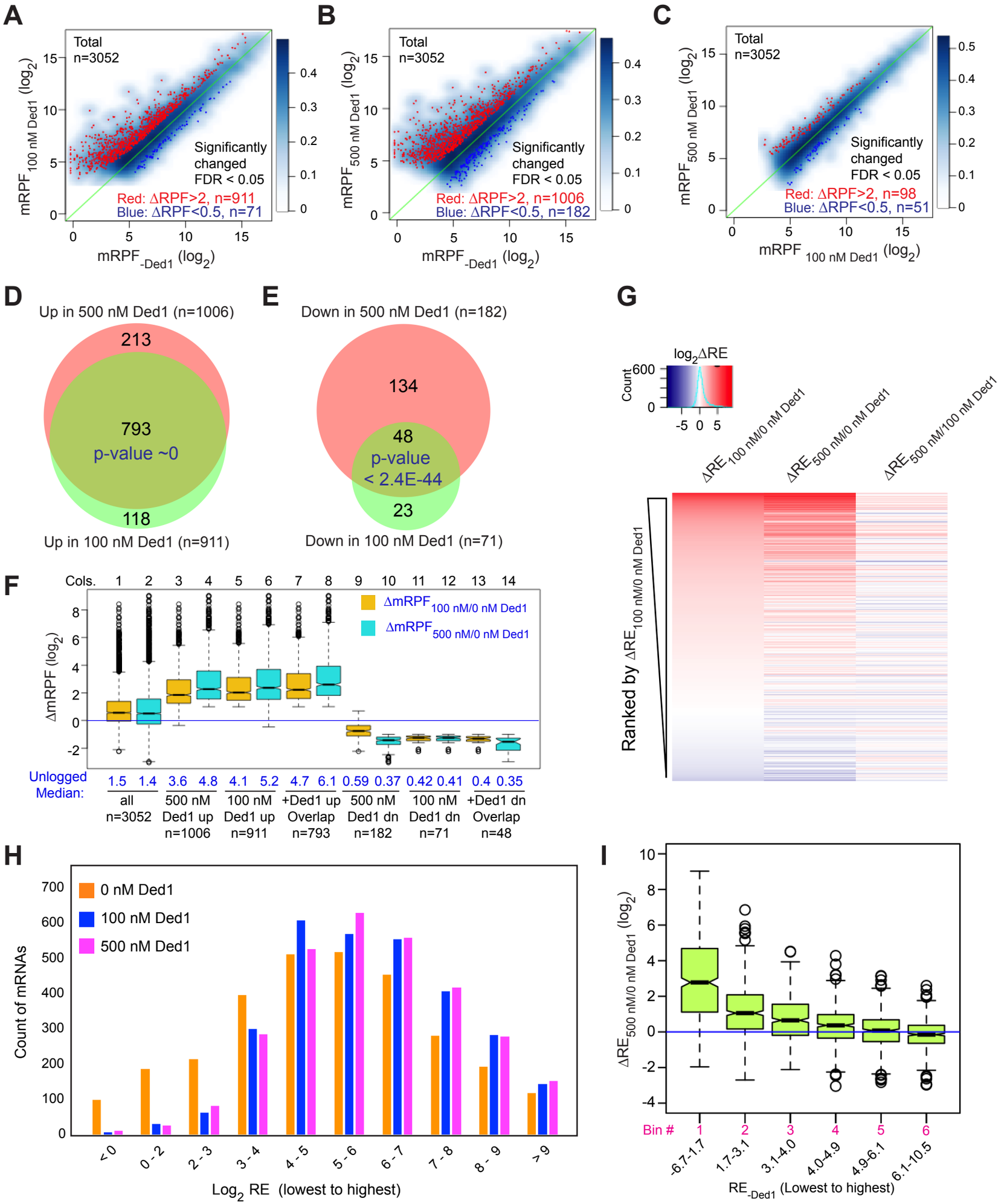
A
Total
n=3052
Significantly changed FDR < 0.05
Red: ΔRPF>2, n=911
Blue: ΔRPF<0.5, n=71
mRPF 100 nM Ded1 (log2)
mRPF -Ded1 (log2)
B
Total
n=3052
Significantly changed FDR < 0.05
Red: ΔRPF>2, n=1006
Blue: ΔRPF<0.5, n=182
mRPF 500 nM Ded1 (log2)
mRPF -Ded1 (log2)
C
Total
n=3052
Significantly changed FDR < 0.05
Red: ΔRPF>2, n=98
Blue: ΔRPF<0.5, n=51
mRPF 500 nM Ded1 (log2)
mRPF 100 nM Ded1 (log2)
D
Up in 500 nM Ded1 (n=1006)
213
793
p-value ~0
118
Up in 100 nM Ded1 (n=911)
E
Down in 500 nM Ded1 (n=182)
134
48
p-value
< 2.4E-44
23
Down in 100 nM Ded1 (n=71)
G
log2ΔRE
Count
600
0
-5 0 5
ΔRE 100 nM/0 nM Ded1
ΔRE 500 nM/0 nM Ded1
ΔRE 500 nM/100 nM Ded1
Ranked by ΔRE 100 nM/0 nM Ded1
F
Cols. 1 2 3 4 5 6 7 8 9 10 11 12 13 14
ΔmRPF 100 nM/0 nM Ded1
ΔmRPF 500 nM/0 nM Ded1
ΔmRPF (log2)
Unlogged Median:
1.5 1.4 3.6 4.8 4.1 5.2 4.7 6.1 0.59 0.37 0.42 0.41 0.4 0.35
all n=3052
500 nM Ded1 up n=1006
100 nM Ded1 up n=911
+Ded1 up Overlap n=793
500 nM Ded1 dn n=182
100 nM Ded1 dn n=71
+Ded1 dn Overlap n=48
H
0 nM Ded1
100 nM Ded1
500 nM Ded1
Count of mRNAs
<0
0 - 2
2 - 3
3 - 4
4 - 5
5 - 6
6 - 7
7 - 8
8 - 9
> 9
Log2 RE (lowest to highest)
I
ΔRE 500 nM/0 nM Ded1 (log2)
Bin # 1 2 3 4 5 6
-6.7-1.7
1.7-3.1
3.1-4.0
4.0-4.9
4.9-6.1
6.1-10.5
RE -Ded1 (Lowest to highest)

Figure 3

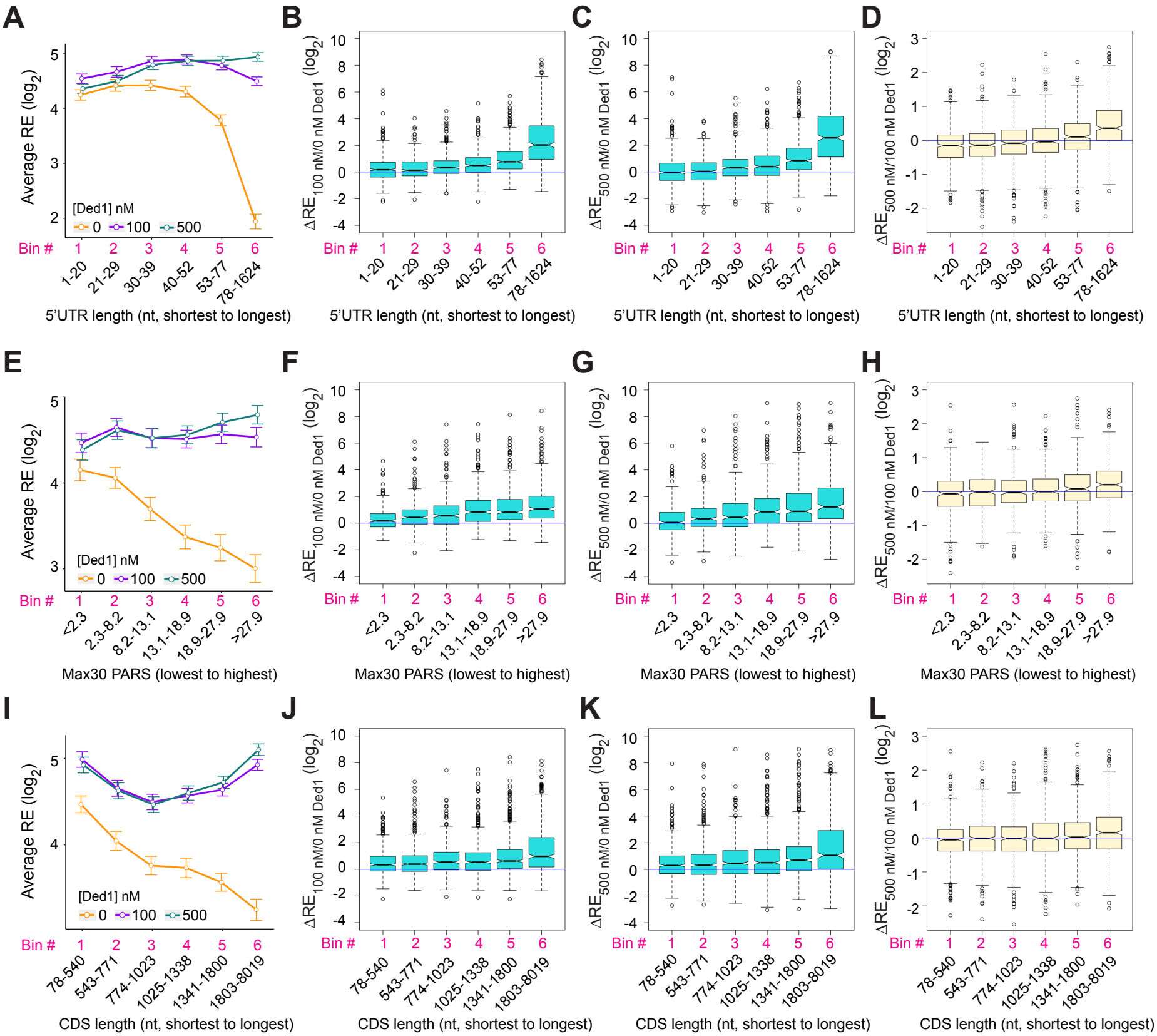
A
B
C
D
E
F
G
H
I
J
K
L
Average RE (log2)
[Ded1] nM
0
100
500
ΔRE100 nM/0 nM Ded1 (log2)
ΔRE500 nM/0 nM Ded1 (log2)
ΔRE500 nM/100 nM Ded1 (log2)
Bin #
1-20
21-29
30-39
40-52
53-77
78-1624
5'UTR length (nt, shortest to longest)
<2.3
2.3-8.2
8.2-13.1
13.1-18.9
18.9-27.9
>27.9
Max30 PARS (lowest to highest)
78-540
543-771
774-1023
1025-1338
1341-1800
1803-8019
CDS length (nt, shortest to longest)

Figure 3-S1

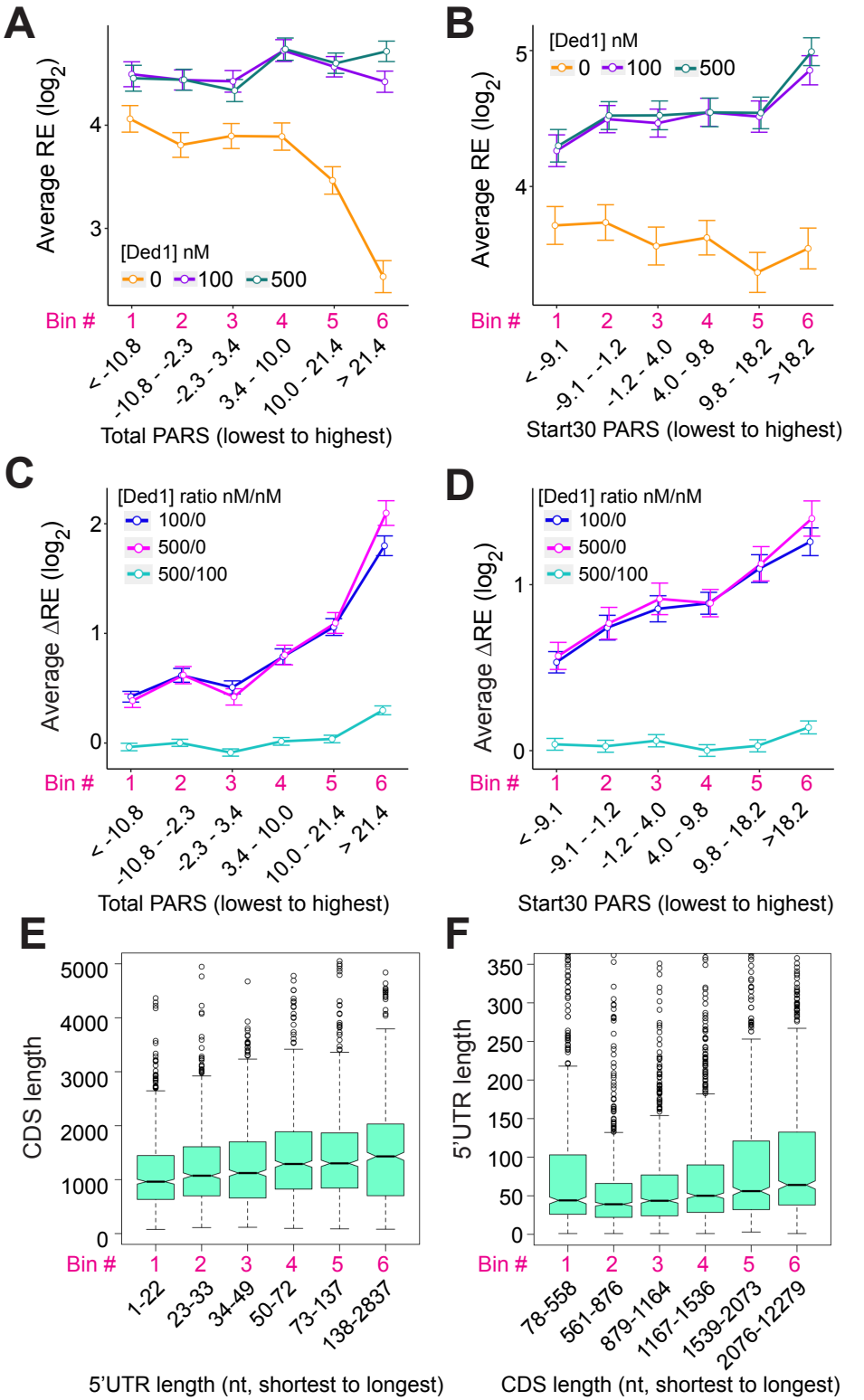
A
Average RE (log2)
[Ded1] nM
0
100
500
Bin #
1
2
3
4
5
6
< -10.8
-10.8 - -2.3
-2.3 - 3.4
3.4 - 10.0
10.0 - 21.4
> 21.4
Total PARS (lowest to highest)
B
Average RE (log2)
[Ded1] nM
0
100
500
Bin #
< -9.1
-9.1 - -1.2
-1.2 - 4.0
4.0 - 9.8
9.8 - 18.2
>18.2
Start30 PARS (lowest to highest)
C
Average ΔRE (log2)
[Ded1] ratio nM/nM
100/0
500/0
500/100
Bin #
Total PARS (lowest to highest)
D
Average ΔRE (log2)
[Ded1] ratio nM/nM
100/0
500/0
500/100
Bin #
Start30 PARS (lowest to highest)
E
CDS length
Bin #
1-22
23-33
34-49
50-72
73-137
138-2837
5'UTR length (nt, shortest to longest)
F
5'UTR length
Bin #
78-558
561-876
879-1164
1167-1536
1539-2073
2076-12279
CDS length (nt, shortest to longest)

Figure 3S-2

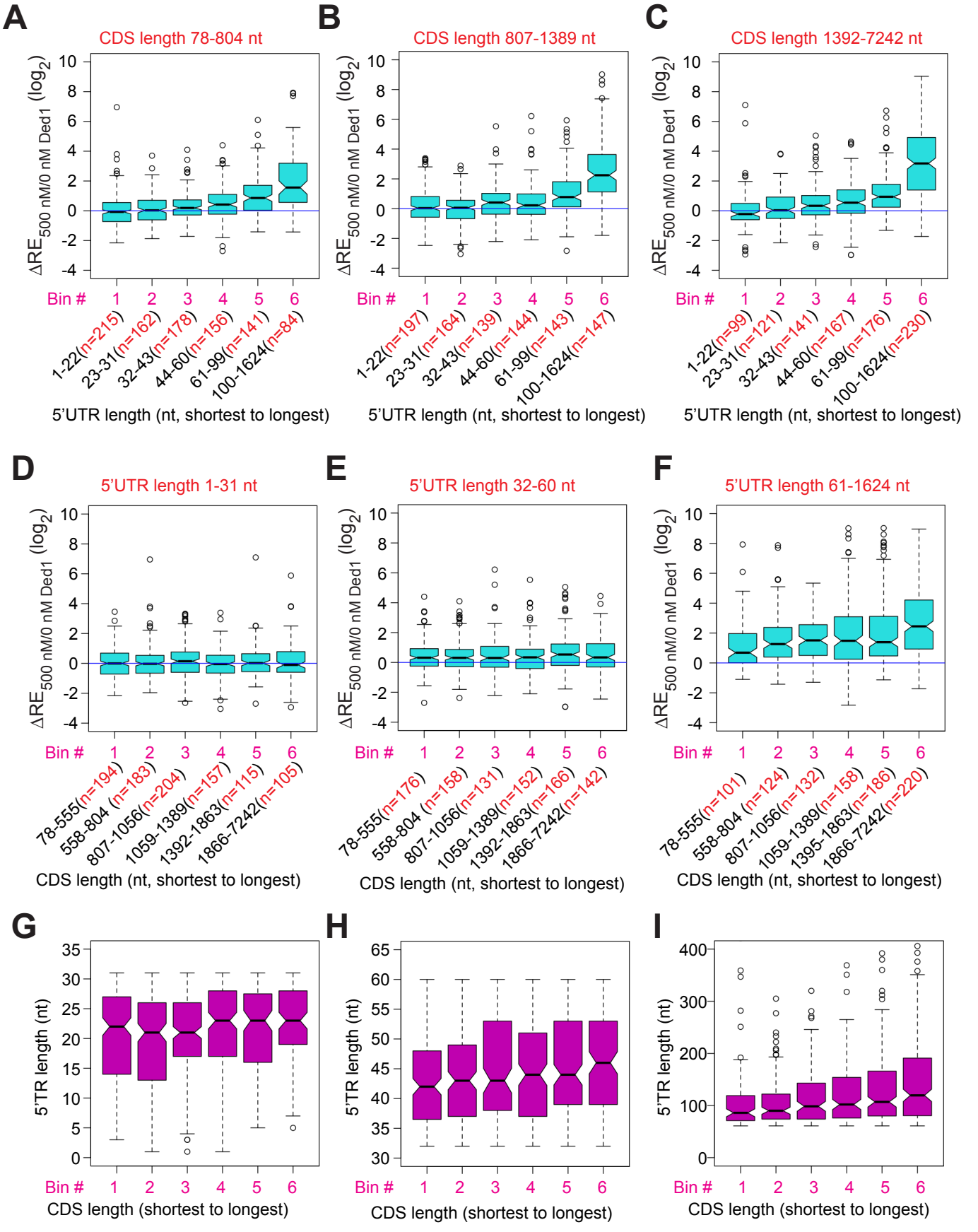
A
CDS length 78-804 nt
B
CDS length 807-1389 nt
C
CDS length 1392-7242 nt
ΔRE500 nM/0 nM Ded1 (log2)
Bin # 1 2 3 4 5 6
1-22(n=215) 23-31(n=162) 32-43(n=178) 44-60(n=156) 61-99(n=141) 100-1624(n=84)
1-22(n=197) 23-31(n=164) 32-43(n=139) 44-60(n=144) 61-99(n=143) 100-1624(n=147)
1-22(n=99) 23-31(n=121) 32-43(n=141) 44-60(n=167) 61-99(n=176) 100-1624(n=230)
5'UTR length (nt, shortest to longest)
D
5'UTR length 1-31 nt
E
5'UTR length 32-60 nt
F
5'UTR length 61-1624 nt
78-555(n=194) 558-804 (n=183) 807-1056(n=204) 1059-1389(n=157) 1392-1863(n=115) 1866-7242(n=105)
78-555(n=176) 558-804 (n=158) 807-1056(n=131) 1059-1389(n=152) 1392-1863(n=166) 1866-7242(n=142)
78-555(n=101) 558-804 (n=124) 807-1056(n=132) 1059-1389(n=158) 1395-1863(n=186) 1866-7242(n=220)
CDS length (nt, shortest to longest)
G
H
I
5'TR length (nt)
CDS length (shortest to longest)

Figure 3-S3

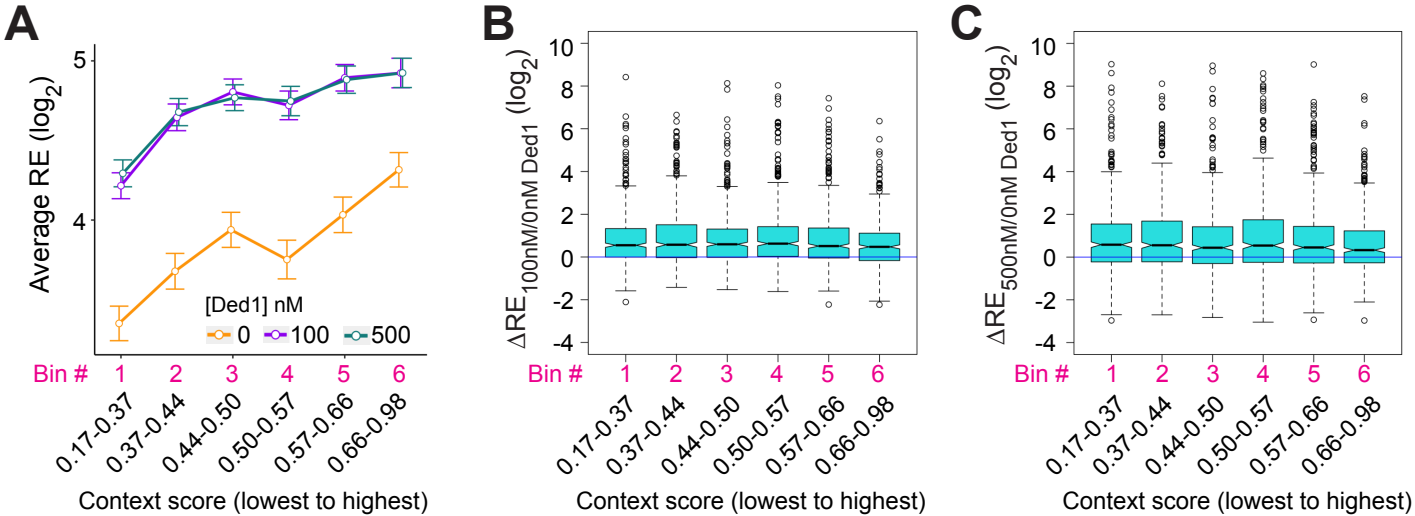
A
Average RE (log2)
5
4
[Ded1] nM
0
100
500
Bin #
1
2
3
4
5
6
0.17-0.37
0.37-0.44
0.44-0.50
0.50-0.57
0.57-0.66
0.66-0.98
Context score (lowest to highest)
B
ΔRE100nM/0nM Ded1 (log2)
10
8
6
4
2
0
-2
-4
Bin #
1
2
3
4
5
6
0.17-0.37
0.37-0.44
0.44-0.50
0.50-0.57
0.57-0.66
0.66-0.98
Context score (lowest to highest)
C
ΔRE500nM/0nM Ded1 (log2)
10
8
6
4
2
0
-2
-4
Bin #
1
2
3
4
5
6
0.17-0.37
0.37-0.44
0.44-0.50
0.50-0.57
0.57-0.66
0.66-0.98
Context score (lowest to highest)

Figure 4

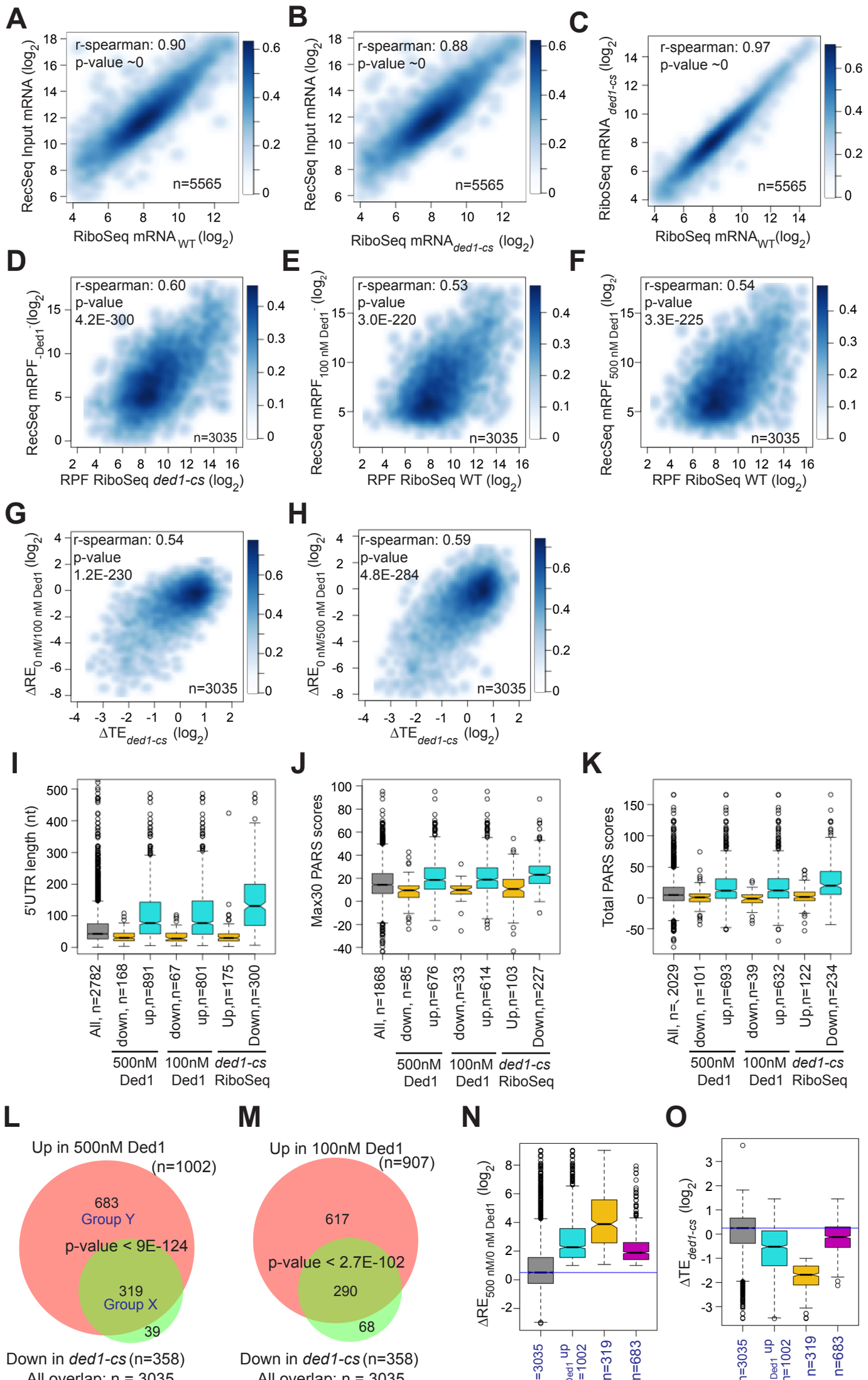
A
r-spearman: 0.90
p-value ~0
n=5565
RecSeq Input mRNA (log2)
RiboSeq mRNA WT (log2)
B
r-spearman: 0.88
p-value ~0
n=5565
RecSeq Input mRNA (log2)
RiboSeq mRNA ded1-cs (log2)
C
r-spearman: 0.97
p-value ~0
n=5565
RiboSeq mRNA ded1-cs (log2)
RiboSeq mRNA WT (log2)
D
r-spearman: 0.60
p-value
4.2E-300
n=3035
RecSeq mRPF -Ded1 (log2)
RPF RiboSeq ded1-cs (log2)
E
r-spearman: 0.53
p-value
3.0E-220
n=3035
RecSeq mRPF 100 nM Ded1 (log2)
RPF RiboSeq WT (log2)
F
r-spearman: 0.54
p-value
3.3E-225
n=3035
RecSeq mRPF 500 nM Ded1 (log2)
RPF RiboSeq WT (log2)
G
r-spearman: 0.54
p-value
1.2E-230
n=3035
ΔRE 0 nM/100 nM Ded1 (log2)
ΔTE ded1-cs (log2)
H
r-spearman: 0.59
p-value
4.8E-284
n=3035
ΔRE 0 nM/500 nM Ded1 (log2)
ΔTE ded1-cs (log2)
I
5'UTR length (nt)
All, n=2782
down, n=168
up,n=891
down,n=67
up,n=801
Up,n=175
Down,n=300
500nM Ded1
100nM Ded1
ded1-cs RiboSeq
J
Max30 PARS scores
All, n=1868
down, n=85
up,n=676
down,n=33
up,n=614
Up,n=103
Down,n=227
500nM Ded1
100nM Ded1
ded1-cs RiboSeq
K
Total PARS scores
All, n=2029
down, n=101
up,n=693
down,n=39
up,n=632
Up,n=122
Down,n=234
500nM Ded1
100nM Ded1
ded1-cs RiboSeq
L
Up in 500nM Ded1
(n=1002)
683
Group Y
p-value < 9E-124
319
Group X
39
Down in ded1-cs (n=358)
All overlap: n = 3035
M
Up in 100nM Ded1
(n=907)
617
p-value < 2.7E-102
290
68
Down in ded1-cs (n=358)
All overlap: n = 3035
N
ΔRE 500 nM/0 nM Ded1 (log2)
all mRNA n=3035
all RE 500nM Ded1 up n=1002
Group X, n=319
Group Y, n=683
O
ΔTE ded1-cs (log2)
all mRNA n=3035
all RE 500nM Ded1 up n=1002
Group X, n=319
Group Y, n=683

Figure 5

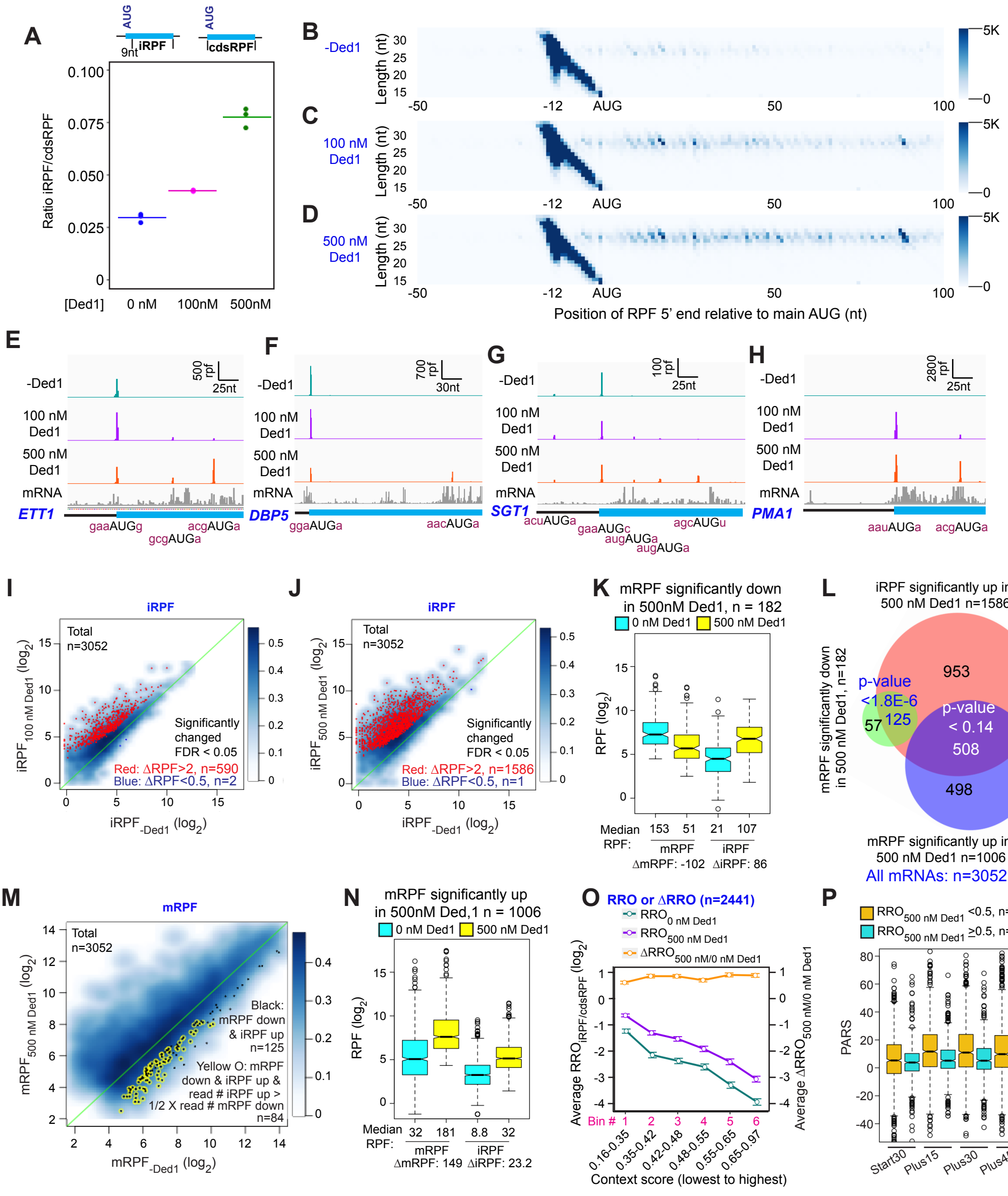
A
AUG
9nt
iRPF
AUG
cdsRPF
Ratio iRPF/cdsRPF
0.100
0.075
0.050
0.025
0
[Ded1]
0 nM
100nM
500nM
B
-Ded1
C
100 nM Ded1
D
500 nM Ded1
Length (nt)
-50
-12
AUG
50
100
5K
0
Position of RPF 5' end relative to main AUG (nt)
E
-Ded1
100 nM Ded1
500 nM Ded1
mRNA
500 rpf
25nt
ETT1
gaaAUGg
gcgAUGa
acgAUGa
F
700 rpf
30nt
DBP5
ggaAUGa
aacAUGa
G
100 rpf
25nt
SGT1
acuAUGa
gaaAUGc
augAUGa
augAUGa
agcAUGu
H
2800 rpf
25nt
PMA1
aauAUGa
acgAUGa
I
iRPF
Total n=3052
Significantly changed FDR < 0.05
Red: ΔRPF>2, n=590
Blue: ΔRPF<0.5, n=2
iRPF100 nM Ded1 (log2)
iRPF-Ded1 (log2)
J
iRPF
Total n=3052
Significantly changed FDR < 0.05
Red: ΔRPF>2, n=1586
Blue: ΔRPF<0.5, n=1
iRPF500 nM Ded1 (log2)
iRPF-Ded1 (log2)
K
mRPF significantly down in 500nM Ded1, n = 182
0 nM Ded1
500 nM Ded1
RPF (log2)
Median RPF:
153
51
21
107
mRPF
iRPF
ΔmRPF: -102
ΔiRPF: 86
L
iRPF significantly up in 500 nM Ded1 n=1586
mRPF significantly down in 500 nM Ded1, n=182
953
p-value <1.8E-6
57
125
p-value < 0.14
508
498
mRPF significantly up in 500 nM Ded1 n=1006
All mRNAs: n=3052
M
mRPF
Total n=3052
Black: mRPF down & iRPF up n=125
Yellow O: mRPF down & iRPF up & read # iRPF up > 1/2 X read # mRPF down n=84
mRPF500 nM Ded1 (log2)
mRPF-Ded1 (log2)
N
mRPF significantly up in 500nM Ded,1 n = 1006
0 nM Ded1
500 nM Ded1
RPF (log2)
Median RPF:
32
181
8.8
32
mRPF
iRPF
ΔmRPF: 149
ΔiRPF: 23.2
O
RRO or ΔRRO (n=2441)
RRO0 nM Ded1
RRO500 nM Ded1
ΔRRO500 nM/0 nM Ded1
Average RROiRPF/cdsRPF (log2)
Average ΔRRO500 nM/0 nM Ded1
Bin #
1
2
3
4
5
6
0.16-0.35
0.35-0.42
0.42-0.48
0.48-0.55
0.55-0.65
0.65-0.97
Context score (lowest to highest)
P
RRO500 nM Ded1 <0.5, n=1054
RRO500 nM Ded1 ≥0.5, n=715
PARS
Start30
Plus15
Plus30
Plus45

Figure 5-S1

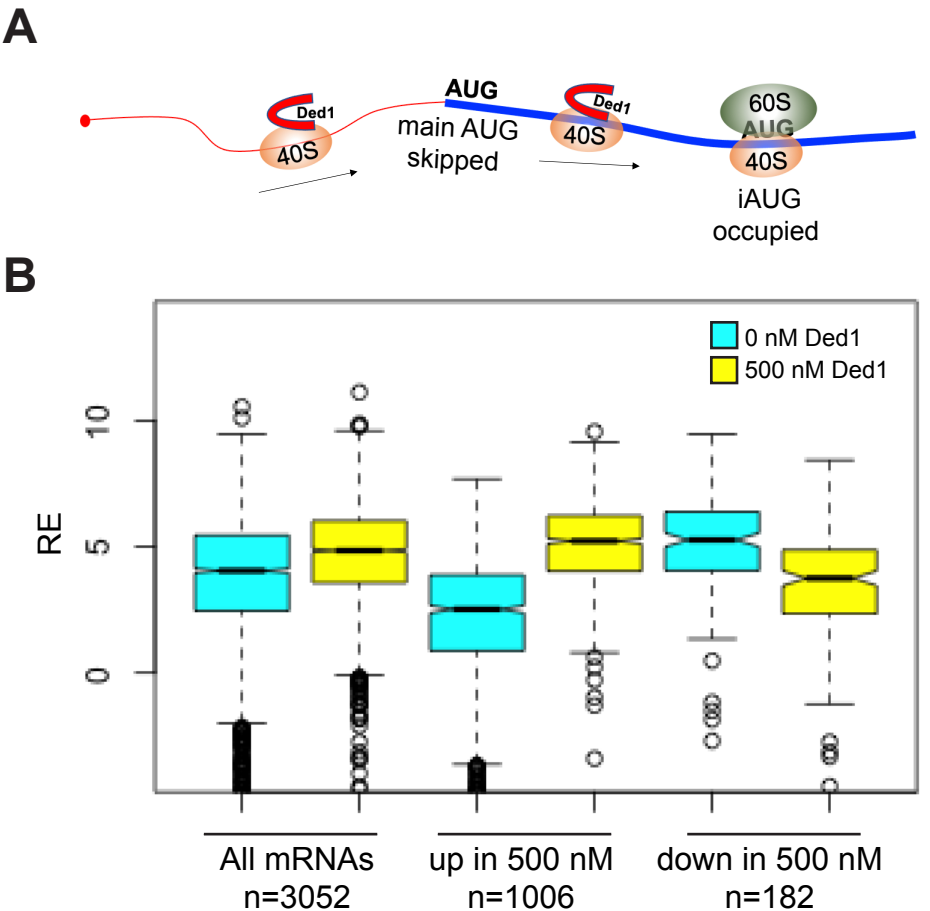
A
Ded1
40S
AUG
main AUG
skipped
Ded1
40S
60S
AUG
40S
iAUG
occupied
B
0 nM Ded1
500 nM Ded1
RE
0
5
10
All mRNAs
n=3052
up in 500 nM
n=1006
down in 500 nM
n=182

Figure 5-S2

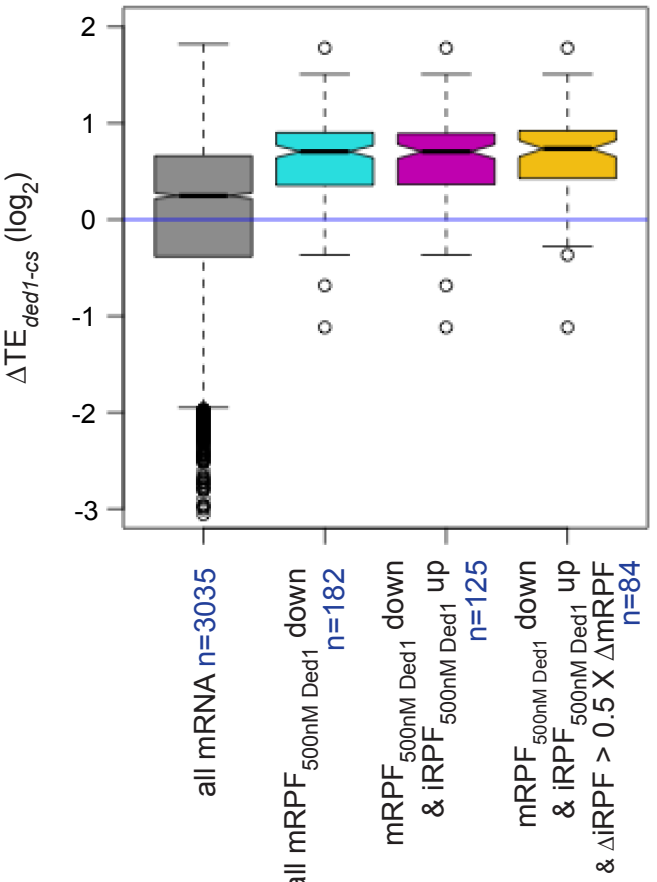
ΔTE$_{ded1\text{-}cs}$ (log$_2$)
2
1
0
-1
-2
-3
all mRNA n=3035
all mRPF$_{500nM\ Ded1}$ down n=182
mRPF$_{500nM\ Ded1}$ down & iRPF$_{500nM\ Ded1}$ up n=125
mRPF$_{500nM\ Ded1}$ down & iRPF$_{500nM\ Ded1}$ up & ΔiRPF > 0.5 X ΔmRPF n=84

Figure 6

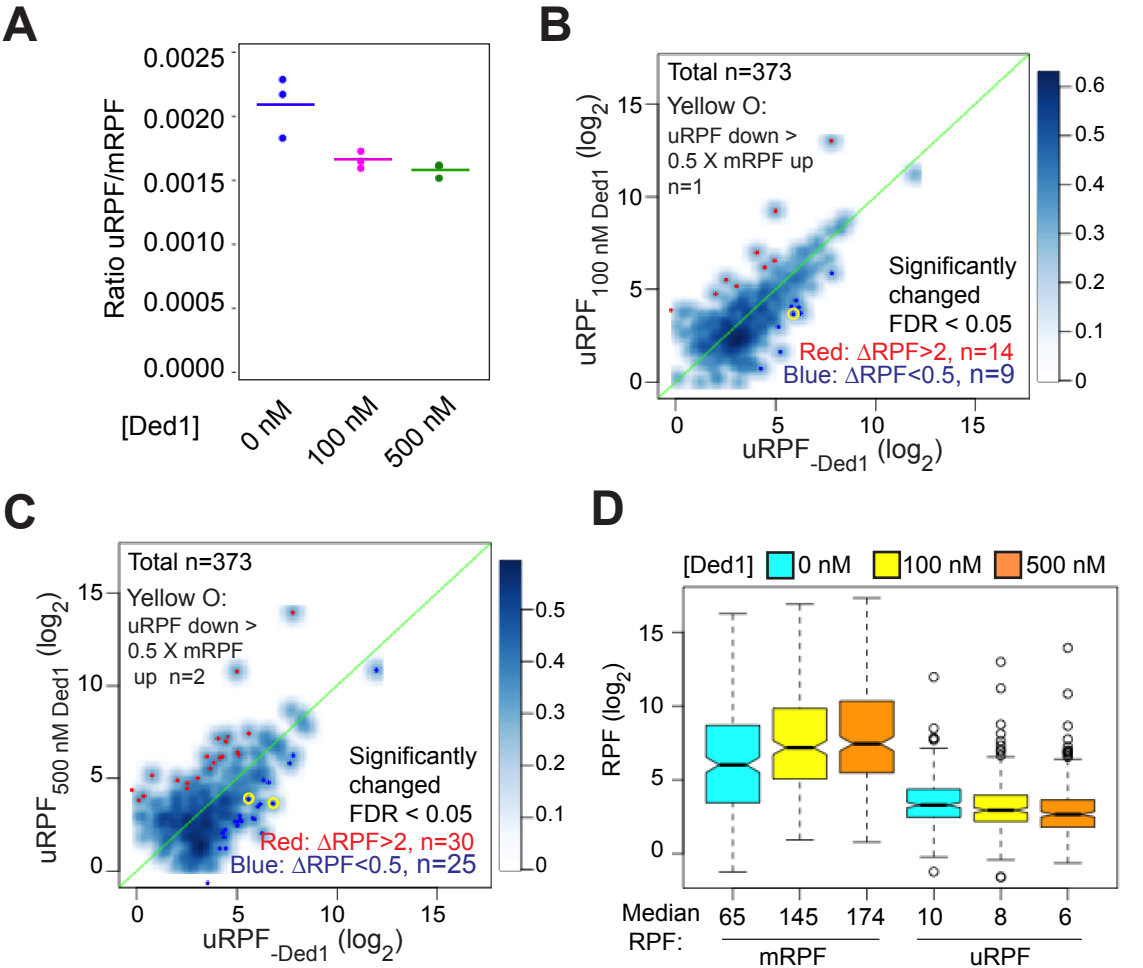
A
Ratio uRPF/mRPF
0.0025
0.0020
0.0015
0.0010
0.0005
0.0000
[Ded1]
0 nM
100 nM
500 nM
B
Total n=373
Yellow O:
uRPF down >
0.5 X mRPF up
n=1
Significantly
changed
FDR < 0.05
Red: ΔRPF>2, n=14
Blue: ΔRPF<0.5, n=9
uRPF 100 nM Ded1 (log2)
uRPF -Ded1 (log2)
C
Total n=373
Yellow O:
uRPF down >
0.5 X mRPF
up n=2
Significantly
changed
FDR < 0.05
Red: ΔRPF>2, n=30
Blue: ΔRPF<0.5, n=25
uRPF 500 nM Ded1 (log2)
uRPF -Ded1 (log2)
D
[Ded1] 0 nM 100 nM 500 nM
RPF (log2)
Median
RPF:
65 145 174 10 8 6
mRPF
uRPF

Figure 6-S1

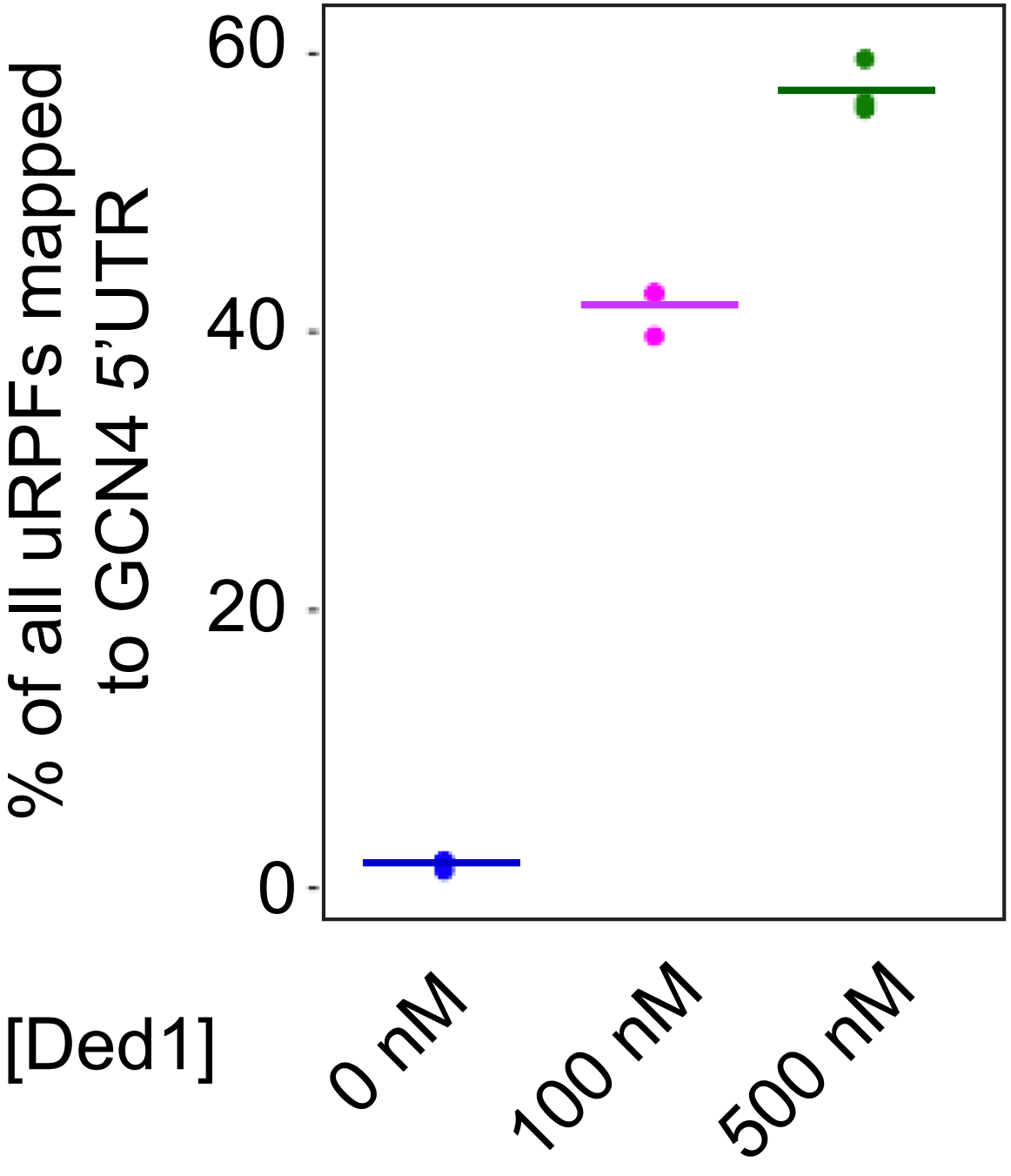
% of all uRPFs mapped to GCN4 5'UTR
60
40
20
0
[Ded1]
0 nM
100 nM
500 nM

Figure 7

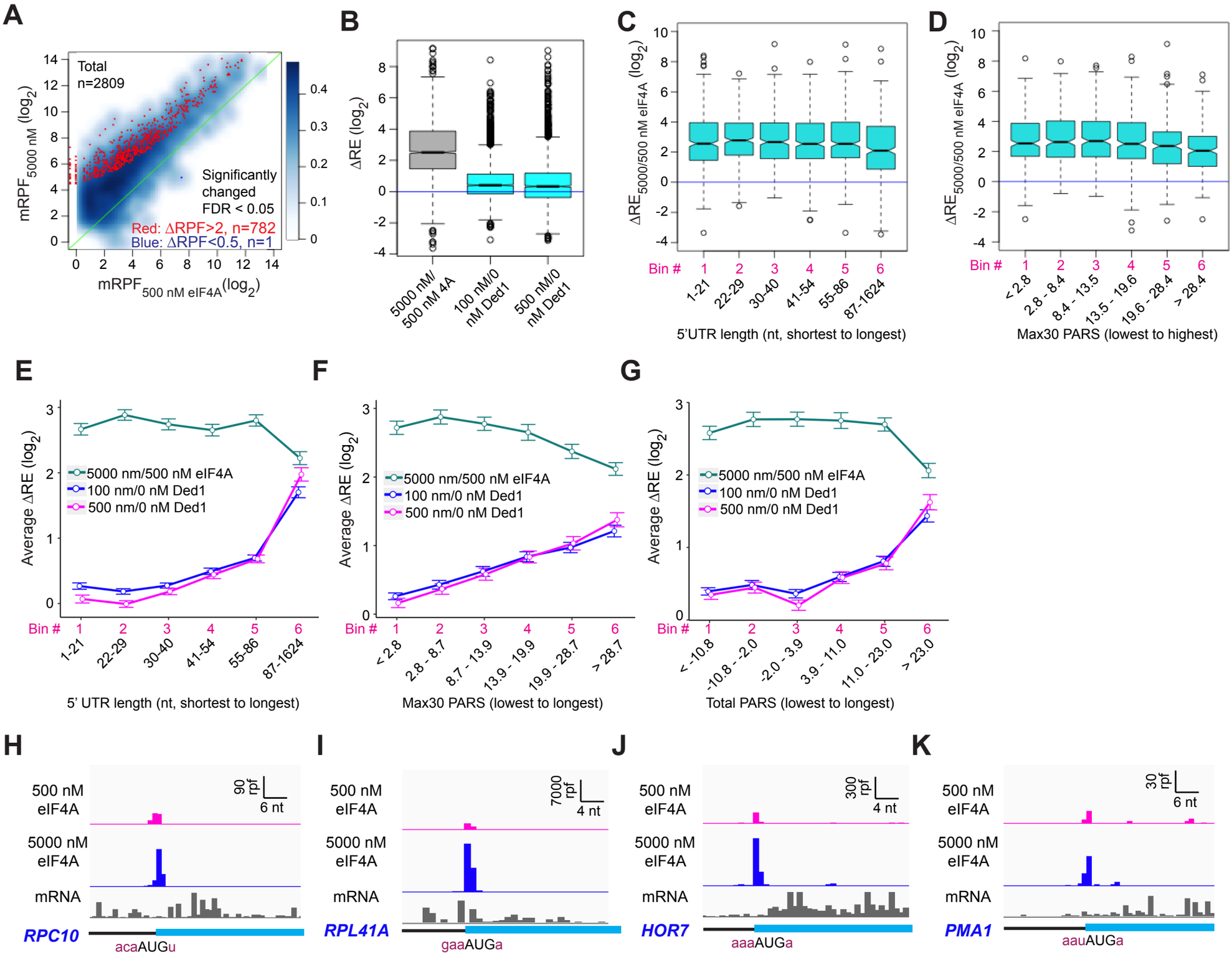
A
Total
n=2809
Significantly changed FDR < 0.05
Red: ΔRPF>2, n=782
Blue: ΔRPF<0.5, n=1
mRPF5000 nM (log2)
mRPF500 nM eIF4A(log2)
B
ΔRE (log2)
5000 nM/ 500 nM 4A
100 nM/0 nM Ded1
500 nM/0 nM Ded1
C
ΔRE5000/500 nM eIF4A (log2)
Bin #
1-21
22-29
30-40
41-54
55-86
87-1624
5'UTR length (nt, shortest to longest)
D
ΔRE5000/500 nM eIF4A (log2)
< 2.8
2.8 - 8.4
8.4 - 13.5
13.5 - 19.6
19.6 - 28.4
> 28.4
Max30 PARS (lowest to highest)
E
Average ΔRE (log2)
5000 nm/500 nM eIF4A
100 nm/0 nM Ded1
500 nm/0 nM Ded1
1-21
22-29
30-40
41-54
55-86
87-1624
5' UTR length (nt, shortest to longest)
F
< 2.8
2.8 - 8.7
8.7 - 13.9
13.9 - 19.9
19.9 - 28.7
> 28.7
Max30 PARS (lowest to longest)
G
< -10.8
-10.8 - -2.0
-2.0 - 3.9
3.9 - 11.0
11.0 - 23.0
> 23.0
Total PARS (lowest to longest)
H
500 nM eIF4A
5000 nM eIF4A
mRNA
90 rpf
6 nt
RPC10
acaAUGu
I
7000 rpf
4 nt
RPL41A
gaaAUGa
J
300 rpf
4 nt
HOR7
aaaAUGa
K
30 rpf
6 nt
PMA1
aauAUGa